A HRH1-YAP1 feedback loop drives pancreatic cancer progression and predicts therapeutic response

JUNLIANG CHEN and JUN WEN

Section for HepatoPancreatoBiliary Surgery, Department of General Surgery, The Third People's Hospital of Chengdu, Chengdu, Sichuan 610014, P.R. China

Received November 11, 2025; Accepted May 15, 2026

DOI: 10.3892/ol.2026.15719

Abstract. Pancreatic ductal adenocarcinoma (PDAC) is a highly lethal malignancy with a dismal prognosis, characterized by an immunosuppressive tumor microenvironment and rapid development of chemoresistance. The present study investigated the histamine receptor H1 (HRH1), a G protein-coupled receptor, and its functional interplay with the transcriptional coactivator YAP1, a known driver of PDAC progression. Through integrated multi-omics analysis of data from TCGA, ICGC and GEO cohorts, the present study found that HRH1 was consistently overexpressed in PDAC, and its expression correlated with poor prognosis. Mendelian randomization analysis further suggested a causal relationship between the use of fexofenadine, an HRH1 antagonist, and a reduced risk of PDAC. Mechanistically, the present study identified a positive feedback loop in which HRH1 stabilizes and activates YAP1 signaling, while YAP1 knockdown downregulates HRH1 transcription, potentially through direct binding to the HRH1 promoter region. The present study constructed a prognostic model based on the HRH1-YAP1 axis by integrating a panel of 101 machine learning algorithms. The model, which includes HRH1, YAP1, ECT2, ITGB5, SHCBP1, MAML2, YWHAZ and ITGA2, effectively stratified patients into groups with differential risk. Patients in the high-risk group exhibited characteristics associated with worse outcomes, including KRAS mutations, chemoresistance, an immunosuppressive microenvironment and reduced responsiveness to immunotherapy. The present study establishes HRH1 as a novel therapeutic target in PDAC and proposes the repurposing of fexofenadine as a promising strategy to disrupt the oncogenic HRH1-YAP1 feedback loop.

Correspondence to: Dr Jun Wen, Section for HepatoPancreatoBiliary Surgery, Department of General Surgery, The Third People's Hospital of Chengdu, 82 Qinglong Street, Chengdu, Sichuan 610014, P.R. China
E-mail: wenjunsyy@163.com

Key words: pancreatic ductal adenocarcinoma, HRH1, YAP1, prognostic model, GPCR, fexofenadine

Introduction

Pancreatic ductal adenocarcinoma (PDAC) is one of the most aggressive solid malignancies, with an overall 5-year survival rate of ~13% in the United States (1,2). Global epidemiological analyses project PDAC to surpass breast and colorectal cancer as the second-leading cause of cancer mortality by 2030 (3). While surgical resection with adjuvant fluorouracil- or gemcitabine-based regimens remains the cornerstone for localized disease, >80% of patients present with unresectable tumors at diagnosis (4). The intractability of PDAC is driven by immunosuppressive stroma, early perineural and vascular metastasis, and rapid development of chemoresistance (5). These factors collectively contribute to PDAC retaining the lowest 5-year relative survival rate among solid tumors, with minimal improvement despite advances in precision medicine.

G protein-coupled receptors (GPCRs) represent the most successful class of druggable targets in biomedicine, with >100 FDA-approved therapeutics modulating GPCR activity (6,7). GPCRs transduce extracellular signals into intracellular responses by activating downstream signaling and transcriptional networks. Their dysregulation drives tumor-promoting processes, including chronic inflammation, metastasis, immune evasion, angiogenesis and chemoresistance (8). Notably, the Rho/ROCK/F-actin pathway, a conserved downstream effector of GPCR activation, serves as a key mechanistic bridge to the Hippo pathway (9). This signaling nexus directly couples GPCR stimulation to the nuclear translocation and transcriptional activity of YAP1.

YAP1, a conserved transcriptional coactivator downstream of the Hippo signaling pathway, orchestrates fundamental physiological processes including cell proliferation, tissue regeneration and organ size control in mammals (10). While oncogenic KRAS mutations initiate >90% of PDAC, previous evidence reveals that the transcriptional coactivator YAP1 not only amplifies KRAS-driven tumor progression through feed-forward signaling loops, but also enables KRAS-independent survival upon therapeutic KRAS suppression (11,12). This functional redundancy underscores a key vulnerability in PDAC biology: Tumors exploit YAP1-mediated transcriptional reprogramming to bypass targeted KRAS inhibition, thereby sustaining proliferation and chemoresistance (13). Thus, delineating the GPCR-YAP1 regulatory axis could inform innovative treatment strategies for this intractable malignancy.

Given the roles of GPCR signaling and YAP1-mediated mechanotransduction in PDAC pathogenesis, the present study aims to elucidate the functional interplay between the GPCR HRH1 and YAP1. We hypothesize that an HRH1-YAP1 regulatory axis underpins tumor progression and therapeutic resistance in PDAC. To elucidate this putative axis, we integrate multi-omics analyses of TCGA, ICGC, and GEO cohorts with experimental validation in cell lines. Furthermore, we employ Mendelian randomization to assess the causal link between HRH1 inhibition and PDAC risk. The present study aimed to construct a machine learning-based prognostic model for refined patient stratification.

Materials and methods

Dataset acquisition. To systematically identify GPCRs associated with pancreatic cancer prognosis, the present study integrated multiple genomic resources. GPCR-related genes were curated from WikiPathways (IDs: WP24, WP58, WP80, WP117, WP247, WP334, WP455, WP501; www.wikipathways.org), while prognostic genes and highly expressed transcripts in pancreatic adenocarcinoma were retrieved from UALCAN (https://ualcan.path.uab.edu) and GEPIA2 (http://gepia2.cancer-pku.cn), respectively (Tables SI-III). Transcriptomic profiles (TPM format), clinical information and somatic mutation data for 178 patients with pancreatic cancer were acquired from TCGA-PAAD cohort using the 'TCGAbiolinks' R package (version 2.36.0; bioconductor.org/). 'TCGAvisualize_oncoprint' function was employed to generate a heatmap illustrating gene mutation frequencies. For independent validation, RNA-seq data and clinical records from the PACA-AU cohort were retrieved from the ICGC database (https://dcc.icgc.org). Raw read counts were converted to TPM values using the 'count2tpm' function in the 'IOBR' package (version 0.99.9; github.com/). Additionally, two microarray datasets (GSE28735 and GSE183795) based on the GPL6244 platform were incorporated to assess the predictive performance of the model (14,15). Clinical metadata and RMA-normalized expression matrices were downloaded from the GEO data portal (https://www.ncbi.nlm.nih.gov/geo). To ensure data comparability, the present study applied rigorous harmonization procedures. All transcriptomic data were log2-transformed [log2(x+1)]. For batch effect correction, the present study used the ComBat algorithm as implemented in the sva R package (v3.56.0, Bioconductor). Specifically, microarray datasets (GSE28735 and GSE183795) were based on RMA-normalized expression matrices, while RNA-seq data from TCGA and ICGC were converted to TPM (Transcripts Per Million) format before log2 transformation and batch correction.

To evaluate the expression profiles of HRH1 in matched tumor and adjacent non-tumor tissue samples, bulk RNA-seq datasets were retrieved from the GEO and ArrayExpress (https://www.ebi.ac.uk/biostudies/arrayexpress) databases, including GSE183795 (85 pairs), GSE62452 (42 pairs), GSE15471 (35 pairs), GSE101448 (18 pairs), GSE16515 (15 pairs), GSE196009 (6 pairs) and E-MTAB-6690 (65 pairs) (14,16-21). Additionally, transcriptomic data from GSE26088 were analyzed to evaluate HRH1 expression across 19 pancreatic cancer cell lines and one normal pancreatic ductal epithelial cell line (HPDE). PL5, also called Panc 04.03, is a pancreatic cancer cell line (https://www.ncbi.nlm.nih.gov/geo/query/acc.cgi?acc=GSM640500; https://www.cellosaurus.org/CVCL_1636). To investigate the regulatory relationship between YAP1 and HRH1 across diverse cancer types, transcriptomic datasets from the GEO were utilized, specifically: Human endothelial cells (GSE211726), breast cancer (GSE59232), neuroblastoma (GSE130401), liver cancer (GSE137915) and renal clear cell carcinoma (GSE146354) (22-25). For single-cell resolution analysis, the CRA001160 dataset containing both normal and pancreatic cancer tissues was employed to compare HRH1 expression across distinct cell populations. Single-cell RNA sequencing data were analyzed with Seurat (v5.3.0; Bioconductor) in R, employing analytical approaches consistent with established protocols (26). Gene expression levels were quantified based on mean unique molecular identifier (UMI) counts.

Tumor mutational burden (*TMB) calculation*. TMB was calculated using somatic mutation data derived from whole-exome sequencing. Specifically, the present study retrieved the harmonized masked somatic mutation data from TCGA database via the 'TCGAbiolinks' R package. To compute TMB, the present study first filtered the mutation annotation format file to retain only protein-altering somatic variants, including missense, non-sense, splice-site and frame-shift indel mutations. Variants classified as germline, silent or located in non-coding regions were excluded. TMB was defined as the total number of qualifying somatic mutations divided by the effective coding region size. Given that TCGA exome capture kits cover ~38 Mb of the coding genome, the present study used this value as the denominator, consistent with prior TCGA-based TMB studies (27,28). TMB values are reported in units of mutations per megabase (mut/Mb), with TMB-high cases defined as those exhibiting ≥10 muts/Mb (29).

Two-sample Mendelian randomization analysis. 'TwoSampleMR' package (version 0.6.14) from the Comprehensive R Archive Network (CRAN, cran.r-project.org/) was used to investigate potential causal relationships between exposure to fexofenadine therapy (GWAS ID: ukb-b-10433; UK Biobank, https://www.ukbiobank.ac.uk/) and pancreatic cancer (GWAS ID: ebi-a-GCST90018893; GWAS Catalog, https://www.ebi.ac.uk/gwas/). Fexofenadine therapy served as the exposure variable. Instrumental variables (IVs) were initially selected using a significance threshold of $P<4.5x10^{-5}$. To mitigate the effects of linkage disequilibrium, IV clumping was performed with an r^2 threshold of 0.001 and a clumping distance cut-off of 10,000 kilobases. Weak IVs, characterized by an F-statistic <10, were subsequently excluded. Given the established associations of obesity, smoking and alcohol consumption with pancreatic cancer risk, IVs potentially associated with these confounding factors were identified through association queries in the GeneAtlas database (geneatlas.roslin.ed.ac.uk/) and subsequently excluded (5). The inverse-variance weighted (IVW) method served as the primary Mendelian randomization (MR) analysis. Secondary MR analyses employed the following methods: MR-Egger regression, weighted median, weighted mode and simple mode. Pleiotropy was assessed using the MR-Egger intercept test. Sensitivity analyses included leave-one-out validation and Cochran's Q statistic to evaluate the heterogeneity among single-nucleotide polymorphisms (SNPs).

Cell culture and transfection. The non-cancerous control cell line hTERT-HPNE (Zhejiang Meisen Cell Technology Co., Ltd.) was cultured in complete DMEM at 37˚C within a humidified atmosphere containing 5% CO_2. The present study obtained all cell culture media, FBS and PDAC cell lines from Procell Life Science & Technology Co., Ltd. Cell lines were cultured under standardized conditions: ASPC1 and BXPC3 in RPMI 1640, CFPAC1 in Iscove's Modified Dulbecco's Medium (IMDM), while PANC1, MIAPaCa-2, Capan-2 and SW1990 were propagated in DMEM.

To knock down target gene expression, transient transfection of siRNAs was carried out with Lipofectamine 3000® (Invitrogen; Thermo Fisher Scientific, Inc.) as per the manufacturer's guidelines. Briefly, 20 μM siRNA duplex was mixed with 6 μl Lipofectamine 3000 in serum-free medium and incubated at room temperature for 15 min to form complexes. The mixture was then added dropwise to cells seeded in 6-well plates containing 2 ml complete growth medium. Cells were maintained at 37˚C for 12 h, after which the transfection medium was replaced with fresh complete medium. Experiments were conducted 48 h post-transfection to allow sufficient knockdown of target genes. The following small interfering (si)RNA duplexes (Shanghai GenePharma Co., Ltd.) were employed: For HRH1 silencing, i) 5'-GGACAAGUGUGAGACAGACTT-3' (sense) and 5'-GUCUGUCUC ACACUUGUCCTT-3' (antisense); ii) 5'-GCUCUGGUUCUAUGCCAAGAU-3' (sense) and 5'-AUCUUGGCAUAGAACCAGAGC-3' (antisense); for YAP1 knockdown, 5'-GUCAGAGAUACUUCUUAAATT-3' (sense) and 5'-UUUAAGAAGUAUCUCUGACTT-3' (antisense). A non-targeting control siRNA (5'-UUCUCCGAACGUGUC ACGUTT-3' (sense) and 5'-ACGUGACACGUUCGGAGAAUT T-3' (antisense) served as a negative control.

Pharmacological modulation of HRH1 activity. Fexofenadine (cat. no. HY-B0801; MedChemExpress) was employed as a selective HRH1 antagonist, while histamine (cat. no. HY-B1204; MedChemExpress) served as the HRH1 agonist.

Cell proliferation assay and cytotoxicity assay. A seeding density of 2,000 cells/well was used in 96-well plates. Following incubation at 37˚C for 2 h, the culture medium was replaced with Cell Counting Kit-8 (CCK-8; cat. no. GK10001; GlpBio Technology) working solution (medium: CCK-8=10: 1) and incubated for 3 h. Absorbance at 450 nm was measured at 24-h intervals for up to 96 h.

For cytotoxicity assessment, tumor cells were seeded at a density of 4,000 cells per well in 96-well plates and cultured at 37˚C for 24 h prior to treatment with gemcitabine. (cat. no. GC16805; GlpBio Technology) at concentrations of $1x10^{-6}$, $1x10^{-3}$, $1x10^{-2}$, $1x10^{-1}$, 1, 10, 100, and 1,000 μM. Following 48 h of drug incubation at 37˚C, optical density (OD) signals were measured. Cell viability was calculated with the formula: Cell viability=(OD of gemcitabine-exposed group-blank OD)/(OD of untreated control group-blank OD). The IC_{50} was determined by non-linear regression analysis using GraphPad Prism (version 9.00; GraphPad Software, Dotmatics).

Reverse transcription-quantitative PCR (RT-qPCR). Total RNA was extracted from cells using the Seven RNAkey Reagent (cat. no. SM139-02; Sevenbio) and reverse transcribed into cDNA with the Sevenbio cDNA Synthesis kit (cat. no. SM135-02), following the manufacturer's protocol. Gene expression analysis was performed on a 7500 Fast Real-Time PCR System (Applied Biosystems; Thermo Fisher Scientific, Inc.) using SYBR Green qPCR MasterMix (Sevenbio). 36B4 (RPLP0) was selected as the internal reference gene for qPCR analysis because it exhibits stable and consistent expression in pancreatic cancer cell lines, which has been widely validated in pancreatic cancer gene expression studies (30-35). CTGF (also known as CCN2) and CYR61 (also known as CCN1) are key downstream effector genes in the YAP1 signaling pathway (36). All primer sequences provided below are presented from the 5' to 3'direction. The primer sequences used for qPCR were as follows: 36B4 forward (F): GCAGCATCTACAACCCTGAAG; 36B4 reverse (R): CAC TGGCAACATTGCGGAC; CYR61 F: CCCGTTTTGGTAGATTCTGG; CYR61 R: GCTGGAATG CAACTTCGG; CTGF F: ACCGACTGGAAGACACGT TTG; CTGF R: CCAGGTCAGCTTCGCAAGG; ANKRD1 F: GTGTAGCACCAGATCCATCG; ANKRD1 R: CGGTGA GACTGAACCGCTAT; YAP1 F: CAGACAGTGGACTAA GCATGAG; YAP1 R: CAGGGTGCTTTGGTTGATAGT A; HRH1 F: GCTGGGCTACATCAACTCCAC; HRH1 R: CCC TTAGGAGCGAATATGCAGAA. The thermocycling conditions were 95˚C for 30 sec (initial denaturation), followed by 40 cycles of 95˚C for 10 sec (denaturation) and 60˚C for 30 sec (annealing/extension). Fluorescence signals were collected during the annealing/extension step. Relative gene expression levels were quantified using the $2^{-\Delta\Delta Cq}$ method, with normalization to the internal reference gene 36B4 to minimize experimental variability (37).

Western blot analysis. Western blotting was performed according to established protocols (38). Briefly, cells were lysed using RIPA buffer (cat. no. SW104-02; Sevenbio) followed by sonication using a JY92-IIN ultrasonic cell disruptor (Ningbo Scientz Biotechnology Co., Ltd.) on ice at 20-25 kHz, 30% output power with cycles of 3 sec pulse and 3 sec interval, repeated for a total of 3 cycles to minimize protein denaturation. The resulting supernatants were collected, quantified using the BCA assay (Sevenbio), and denatured with 5x loading buffer (Beyotime Biotechnology). Protein samples containing 20 μg of total protein per lane were separated by SDS-PAGE using 7.5% polyacrylamide resolving gels. Following electrophoresis and transfer, PVDF membranes (MilliporeSigma) were blocked with 5% non-fat milk at room temperature for 2 h, then incubated with primary antibodies overnight at 4˚C. Primary antibodies against YAP1 (1:10,000; cat no. 13584-1-AP) and β-actin (1:10,000; cat no. 66009-1-Ig) were purchased from Proteintech Group, Inc., with β-actin used as the loading control for normalization. After washing, the membranes were incubated for 2 h at room temperature with the appropriate HRP-conjugated secondary antibody (Proteintech Group, Inc.) diluted 1:100,000. Specifically, goat anti-mouse IgG (cat. no. SA00001-1) was used for mouse primary antibodies, while goat anti-rabbit IgG (cat. no. SA00001-2) was employed for rabbit primary antibodies. This was followed by protein band detection using an enhanced chemiluminescence detection kit from Beyotime Biotechnology and imaging with the ImageQuant 800 system (Cytiva).

ChIP-Atlas database analysis. Here, YAP1 ChIP-seq, H3K4me3, H3K27ac and ATAC-seq datasets were retrieved from the ChIP-Atlas database (chip-atlas.org/) to investigate the binding sites of YAP1 at the HRH1 promoter region. Based on the GENCODE database (GRCh38 assembly; https://www.gencodegenes.org/human/), the HRH1 RefSeq sequence is located on chromosome 3 at position 11,154,493-11,263,557 (https://genome.ucsc.edu/cgi-bin/hgSearch?search=HRH1&db=hg38). The downloaded BigWig files were visualized using the 'Integrative Genomics Viewer' (IGV; version 2.19.4; Broad Institute), with detailed dataset identifiers and download links provided in Table SIV. Since the ChIP-seq data presented in the present study were obtained exclusively from the ChIP-Atlas database, none of the cell lines were cultured or experimentally manipulated in the present study. Notably, the 'PCa3' in Table SIV refers to patient-derived prostate cancer organoids, which are well-characterized models derived from advanced prostate cancer metastases (39,40). Their genomic characterization (copy number alterations, mutations) and functional data are publicly accessible via the MSKCC cBioportal (http://www.cbioportal.org) and the NCBI PMC repository (pmc.ncbi.nlm.nih.gov/articles/PMC4237931/).

Enrichment analysis. Pathway enrichment patterns were evaluated through GSEA implemented in the clusterProfiler R package (version 4.16.0; Bioconductor), analyzing transcriptomic data from TCGA-PAAD cohort (41). The Molecular Signatures Database was utilized to acquire predefined gene signatures, specifically the Cordenonsi_YAP_Conserved (M2871) and YAP1_UP (M2845) gene sets. Patients were stratified into high- and low-expression groups based on HRH1 levels and differentially expressed genes (DEGs) were identified using the 'limma' package (version 3.21, Bioconductor). The false discovery rate (FDR) was used for multiple-testing correction, with thresholds of FDR<0.05 and |log2FC|>1. Functional annotation of DEGs was conducted using Metascape (https://metascape.org/) to elucidate enriched biological pathways.

Chemotherapy response prediction. To predict chemosensitivity in TCGA-PAAD cohort, the present study employed the 'oncoPredict' R package (version 1.2; CRAN), a computational tool that integrates genomic features with drug response profiles (42). Training data were derived from the Cancer Cell Line Encyclopedia (CCLE; https://sites.broadinstitute.org/ccle/) and the Cancer Therapeutics Response Portal (CTRP; https://portals.broadinstitute.org/ctrp/), enabling the calculation of chemotherapy resistance scores for each patient.

Tumor microenvironment (TME) characterization and immunotherapy response prediction. The cellular composition of the TME was analyzed using the 'deconvo_tme' function within the 'IOBR' R package (43). This module integrates six well-established, publicly available deconvolution algorithms for the inference of cellular abundances from bulk transcriptomic data: CIBERSORT, MCP-counter, EPIC, xCell, quantTIseq and TIMER (44-49).

Furthermore, ssGSEA was performed to compute cellular enrichment scores for each patient using the 'calculate_sig_score' algorithm (50). Gene reference sets utilized for ssGSEA quantification were derived from authoritative literature (51-55). The TIDE computational method was employed to calculate the Immune Checkpoint Inhibitor (ICI) resistance score (55). Patients exhibiting high TIDE scores demonstrate susceptibility to immune evasion and exhibit lower response rates to immunotherapy.

Machine learning-based prognostic model construction. To develop a robust and generalizable prognostic signature, the present study utilized the OmniLearn R package, which facilitates automated model construction across distinct machine learning algorithms (https://github.com/Feng-Rommel/OmniLearn). In line with previous reports (56), the present study implemented 101 specific algorithmic configurations (Table SV) to establish the prognostic model. These configurations were derived from 10 core survival modeling methods: Random Survival Forest (RSF), CoxBoost, stepwise Cox regression, Lasso, Ridge, Elastic Net (Enet), Survival Support Vector Machines (survival-SVM), Generalized Boosted Regression Modeling (GBM), Supervised Principal Components (SuperPC) and Partial Least Squares Cox regression (plsRcox). Models were established using single algorithms or paired combinations. In the combined strategy, genes were initially screened using the 'RunML' function (mode: 'Variable'). Algorithms yielding <3 candidate features were excluded from further modeling, while those with ≥3 features proceeded to model construction using the 'RunML' function (mode: 'Model'). Single-method models were constructed directly using the 'RunML' function (mode: 'Model').

Specific parameter settings for these ten core algorithms are described below. For stepwise Cox regression, all three directionality strategies ('forward', 'backward' and 'both') were tested. Penalized regression models (Lasso, Ridge, Enet) were fitted using the 'glmnet' package via the 'cv.glmnet' function, with the regularization parameter λ tuned through 10-fold cross-validation (CV). The elastic net mixing parameter α was systematically swept from 0 to 1 in increments of 0.1 (α=0: Ridge; α=1: Lasso; 0<α <1: Enet). Survival-SVM was implemented using the 'survivalsvm' package. GBM models were trained with the 'gbm' package under ten-fold CV. SuperPC, an extension of PCA adapted for survival outcomes, was executed via the 'superpc' package, with tuning performed using the 'superpc.cv' function (ten-fold CV). The plsRcox model was optimized using the 'cv.plsRcox' function from the 'plsRcox' package. Finally, RSF was implemented with the 'randomForestSRC' package using the 'rfsrc' function, fixing ntree to 500 and nodesize to 5 based on empirical validation to balance computational efficiency and predictive stability.

Following the construction of distinct prognostic models using TCGA-PAAD dataset (n=178) as the training set, risk scores for both the training cohort (TCGA-PAAD) and an external validation cohort (ICGC-PACA-AU; n=95) were calculated using the 'CalPredictScore' function. Subsequently, model performance was evaluated by computing the C-index via the 'RunEval' function. To ensure robustness, the optimal model was selected based on the highest mean C-index across both TCGA-PAAD and ICGC-PACA-AU cohorts. Finally, two microarray datasets (GSE28735 and GSE183795) were merged to constitute an additional external validation set (14,15).

Time-dependent calibration was assessed using the Brier score at 1-4 years via the 'pec' package (Version 2025.06.24). This machine learning framework enables unbiased identification of robust prognostic biomarkers while mitigating overfitting through ensemble-based feature selection.

Statistical analysis. Uni- and multivariate Cox proportional hazards regression analyses, Kaplan-Meier (KM) curve generation and log-rank testing for survival differences were performed using the 'survival' (version 3.8-3; CRAN) and 'survminer' (version 0.5.1; CRAN) packages. Principal component analysis (PCA) was implemented via the 'stats' package and time-dependent receiver operating characteristic (ROC) evaluation was conducted using the 'timeROC' package (version 0.4; CRAN). For comparisons involving only two groups, unpaired Student's t-test or the Wilcoxon rank-sum test was used, as appropriate. When a single control group was compared against multiple treatment groups, statistical significance was assessed by one-way ANOVA followed by Dunnett's post hoc test. The correlation between two variables was investigated using a non-parametric Spearman test. All statistical tests are two-tailed. Data from experiments are presented as mean ± standard deviation (SD). All statistical analyses were performed in R (version 4.5.1), and $P<0.05$ was considered to indicate a statistically significant difference.

Results

Expression and prognostic significance of HRH1 in pancreatic cancer. To identify potential therapeutic targets for PDAC, the present study intersected three gene sets: 381 GPCR genes, 1,285 genes significantly associated with prognosis (log-rank $P<0.01$) in TCGA-PAAD cohort and 2,456 genes markedly upregulated ($log_2FC >2$) in PDAC from the same cohort. This analysis yielded two candidate genes, GPRC5A and HRH1 (Fig. 1A). Due to the lack of specific pharmacological agents targeting GPRC5A, HRH1 was chosen as the main focus of this investigation because it has targeted inhibitors (57).

KM analysis in TCGA-PAAD cohort revealed that high expression of HRH1 was significantly associated with unfavorable overall survival (Fig. 1B). Both univariate and multivariate Cox regression analyses further identified HRH1 as an independent prognostic factor in pancreatic cancer (Fig. S1). Analysis using the GEPIA2 online platform confirmed significant overexpression of HRH1 in PDAC samples (Fig. 1C). Moreover, bulk RNA sequencing of 266 matched patient samples across seven independent cohorts demonstrated consistently higher HRH1 expression in tumor tissues relative to adjacent non-tumor counterparts (Fig. 1D). Analysis of the GSE26088 dataset revealed that HRH1 expression was elevated across 19 pancreatic cancer cell lines relative to the normal pancreatic ductal epithelial cell line HPDE (Fig. 1E). qPCR validated increased HRH1 expression in seven PDAC cell lines compared with the non-cancerous HPNE cell line (Fig. 1F). At single-cell resolution, malignant cells exhibited higher average UMI counts for HRH1 than normal ductal cells (Fig. 1H).

HRH1 as a druggable vulnerability in PDAC. TMB analysis suggested a positive association between high HRH1 expression and increased mutation load (Fig. 1G). Evaluation using the 'TIDE' algorithm revealed a positive association between HRH1 expression and TIDE score, implying that high HRH1 expression may be associated with diminished ICI efficacy (Fig. 1I). Additionally, chemoresistance prediction analysis indicated that high HRH1 expression (stratified by median expression) was associated with resistance to multiple chemotherapeutic agents, including gemcitabine, fluorouracil, SN-38, oxaliplatin, doxorubicin, platinum-based drugs, mitomycin and vincristine (Figs. 1J-M, S2).

To further investigate the potential therapeutic relevance of HRH1 in PDAC, the present study performed MR analysis. The IVW method indicated that fexofenadine treatment is associated with a reduced risk of pancreatic cancer ($OR=1.71x10^{-20}$; Figs. 2A, 3A; Table SVI). Leave-one-out sensitivity analysis confirmed the robustness of these findings (Fig. 2B). The analysis showed no significant heterogeneity (MR-Egger $Q=9.224$) and no evidence of horizontal pleiotropy (Fig. S3B; Table SVII).

Following HRH1 knockdown using siRNA, the proliferation of PANC-1 and SW1990 cells was inhibited compared with control cells (Fig. 2C and D). In PANC1 cells, silencing HRH1 enhanced sensitivity to gemcitabine (Fig. 2E). The IC_{50} for the siControl group was 163.9 μM, whereas it was markedly reduced to 8.226 μM and 3.645 μM in the siHRH1#1 and siHRH1#2 groups, respectively (Fig. 2E). A similar potentiation of gemcitabine cytotoxicity was observed in SW1990 cells upon HRH1 knockdown. The IC_{50} value for the siControl group was 3.827 μM, which decreased to 0.2241 μM and 0.09096 μM in the siHRH1#1 and siHRH1#2 groups, respectively (Fig. 2F). The RT-qPCR validation data for HRH1 knockdown efficiency are provided in Fig. 3E and F. Collectively, these results underscore HRH1 as a promising therapeutic target in pancreatic cancer.

Positive feedback loop between HRH1 and YAP1. To investigate the signaling pathways activated by HRH1 in PDAC, the present study divided samples into high and low expression groups based on the median expression of HRH1 and identified DEGs between the two groups. Metascape enrichment analysis revealed that upregulated DEGs in the high HRH1 expression group were associated with YAP1 signaling (Fig. 3A). GSEA analysis indicated a positive correlation between HRH1 and the 'Cordenosi YAP conserved signature' as well as the 'YAP1 up signature' (Fig. 3B and D). In TCGA-PAAD cohort, HRH1 expression showed a positive correlation with the expression of multiple target genes of the YAP1 signaling pathway (Fig. 3C). Knockdown of HRH1 in human endothelial cells downregulated multiple YAP1 target genes, including CCN1 and CCN2 (Fig. S4A). These results indicated that HRH1 promotes activation of the YAP1 signaling pathway in endothelial cells. In PANC1 and SW1990 cells, knockdown of HRH1 resulted in decreased expression of CTGF, CYR61 and ANKRD1, while the transcriptional levels of YAP1 remained largely unchanged (Fig. 3E and F), indicating that HRH1 may influence YAP1 pathway activity by affecting YAP1 protein stability rather than its transcription in pancreatic cancer cells. Furthermore, in breast cancer (MDA-MB-231; GSE59232), neuroblastoma (NLF; GSE130401), liver cancer (HepG2; GSE137915), and renal clear cell carcinoma (RCC4; GSE146354), silencing YAP1 led to a significant decrease in HRH1 expression at the transcriptome level (Fig.

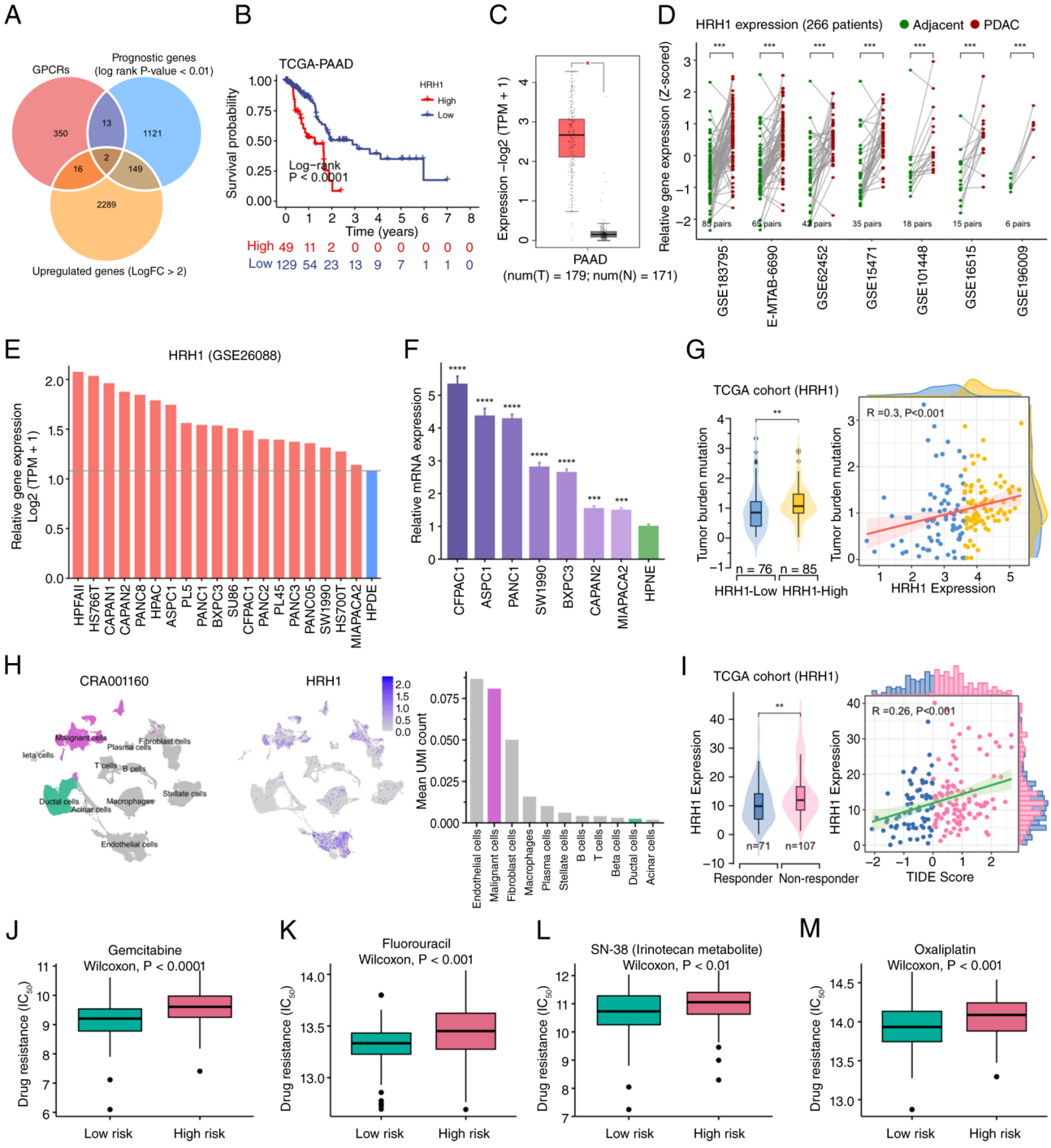

Figure 1. HRH1 is associated with prognosis, chemotherapy resistance and immunotherapy resistance in PDAC. (A) Venn analysis identified GPCR-related genes that are highly expressed and associated with prognosis in PDAC. (B) Kaplan-Meier analysis indicated the prognostic value of HRH1. (C) Online analysis using the GEPIA2 database showed HRH1 expression in pancreatic cancer and normal tissue (one-way ANOVA; *P<0.05). (D) HRH1 expression in tumor tissues and matched adjacent normal tissues. Data were obtained from 266 patients across seven cohorts (Wilcoxon rank-sum test; ***P<0.001). (E) Sequencing data from GSE26088 revealed that HRH1 expression was higher in 19 pancreatic cancer cell lines when compared with the normal pancreatic cell line (HPDE). (F) Reverse transcription quantitative-PCR analysis of HRH1 expression. Each of the 7 PDAC cell lines was compared with the control HPNE cell line. Statistical significance was assessed by one-way ANOVA followed by Dunnett's post hoc test (****P<0.0001; ***P<0.001). (G) Relationship between HRH1 expression and tumor mutation burden (Wilcoxon rank-sum test; **P<0.01). (H) In the CRA001160 dataset, HRH1 expression across different cell types, displayed using UMAP plot, feature plot and bar plot reflecting mean UMI count. (I) Relationship between HRH1 expression and TIDE score (Wilcoxon rank-sum test, **P<0.01). Association between HRH1 expression and resistance to (J) Gemcitabine, (K) Fluorouracil, (L) SN-38 and (M) Oxaliplatin. Statistical comparisons were performed using the Wilcoxon rank-sum test. GPCRs, G protein-coupled receptors; PDAC, pancreatic ductal adenocarcinoma; UMAP, Uniform Manifold Approximation and Projection.

S4B-E). Similarly, through qPCR experiments, it was confirmed that knockdown of YAP1 in PANC1 and SW1990 cells led to decreased expression of HRH1 mRNA (Fig. 3E and F).

YAP1 is a transcriptional co-activator that binds to TEA domain transcription factors (TEAD) proteins and anchors to the promoter regions of target genes to regulate downstream

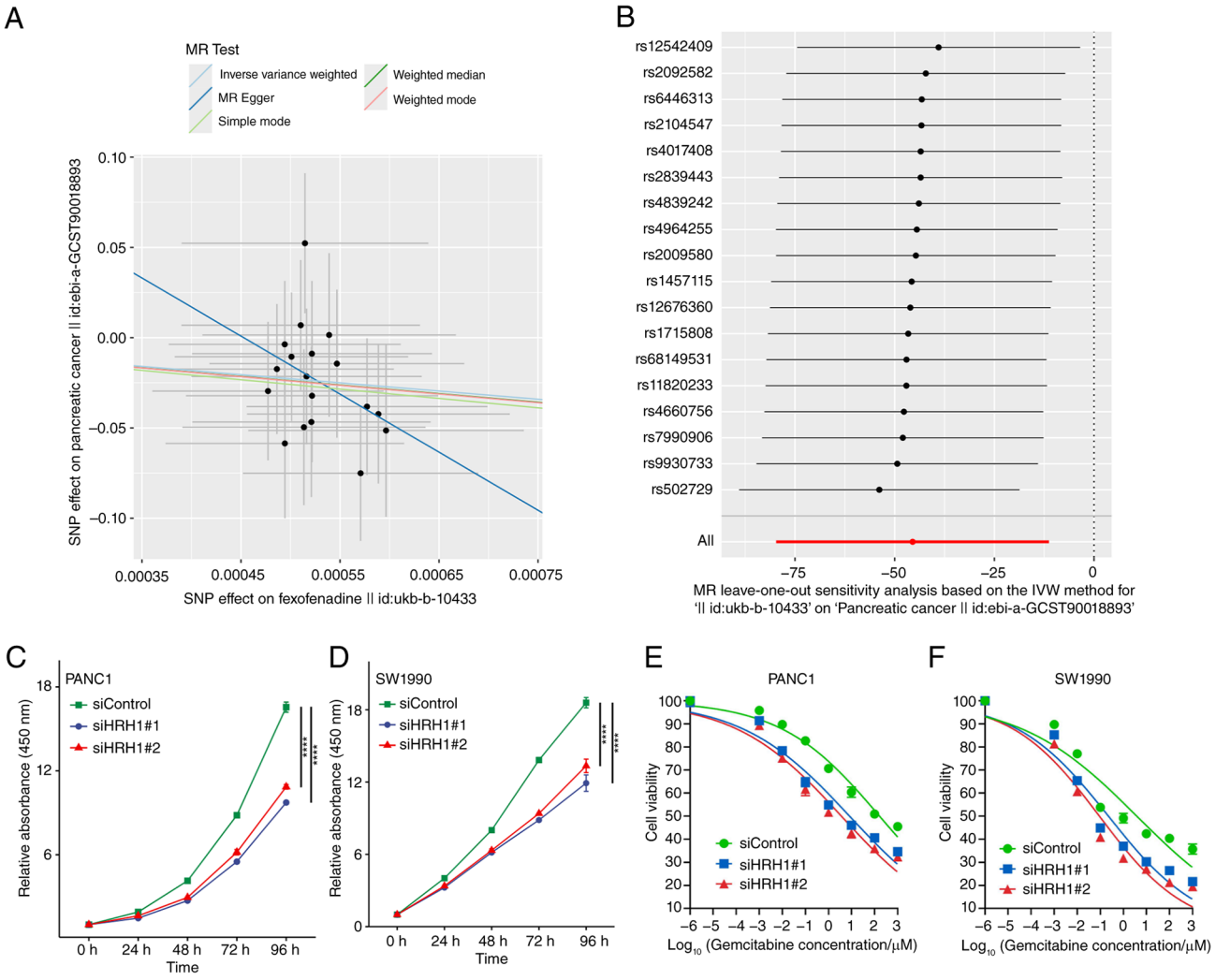

Figure 2. Targeting and inhibiting HRH1 is a potential therapeutic strategy for PDAC. (A) Scatter plot of the causal association between fexofenadine treatment and PDAC. (B) Leave-one-out sensitivity analysis using the IVW method. CCK-8 proliferation assay was used to detect the proliferation of (C) PANC1 cells and (D) SW1990 cells after HRH1 knockdown. The knockdown groups were compared with the non-targeting control in PANC-1 and SW1990 cells. Statistical significance was assessed by one-way ANOVA followed by Dunnett's post hoc test (****P<0.0001). Experiments were performed in triplicate. The reverse transcription-quantitative PCR validation data for HRH1 knockdown efficiency is provided in Fig. 3E and F. Dose-response curves of (E) PANC1 and (F) SW1990 cells transfected with siControl, siHRH1#1 or siHRH1#2 and treated with increasing concentrations of gemcitabine for 48 h. Cell viability was assessed by CCK-8 assay and normalized to the untreated control. PDAC, pancreatic ductal adenocarcinoma; CCK-8, Cell Counting Kit-8; si, small interfering; IVW, inverse variance-weighted.

expression (58). Further analysis using ChIP-Atlas data indicated enrichment of H3K4me3 (an active promoter marker) and H3K27ac (an enhancer/promoter marker) in the genomic region ~1,000 bp upstream of the HRH1 transcription start site (59,60). This region also exhibited high signal in ATAC-seq (open chromatin), suggesting it is likely the promoter region of HRH1 (Fig. 4A). YAP1 ChIP-seq data revealed peaks in the HRH1 promoter region, indicating direct binding of YAP1 to the HRH1 promoter (Fig. 4A). In PA-TU-8902 (pancreatic cancer cells) and PCa3 (prostate cancer cells), knockdown of YAP1 and TAZ led to reduced chromatin accessibility in the HRH1 promoter region (Fig. 4B). Notably, although not all cell lines in Fig. 4A and B are pancreatic cancer-derived, YAP1 binding to the HRH1 promoter was consistently detected across these diverse cell types, indicating that this regulatory mechanism is broadly active across multiple human cancer types and not restricted to pancreatic cancer cells.

GPCR activation transmits signals through the Rho/ROCK/F-actin pathway, thereby regulating YAP1 activity (61). Western blot analysis showed that knockdown of HRH1 in PANC1 and SW1990 cells decreased YAP1 protein expression levels (Fig. 4C and D; Table SVIII). Moreover, inhibition of HRH1 with fexofenadine decreased YAP1 expression compared with the control group, while activation of histamine receptors with histamine increased YAP1 expression. Co-treatment with fexofenadine and histamine also led to decreased YAP1 expression, though to a lesser extent than with fexofenadine alone (Fig. 4E and F; Table SIX). Taken together, these findings indicate that HRH1 stabilizes and activates YAP1 signaling, whereas YAP1 knockdown downregulates HRH1 transcription, potentially through direct binding to the HRH1 promoter region.

Development of a prognostic model based on HRH1/YAP1 signaling. Given the key role of the HRH1/YAP1 signaling axis

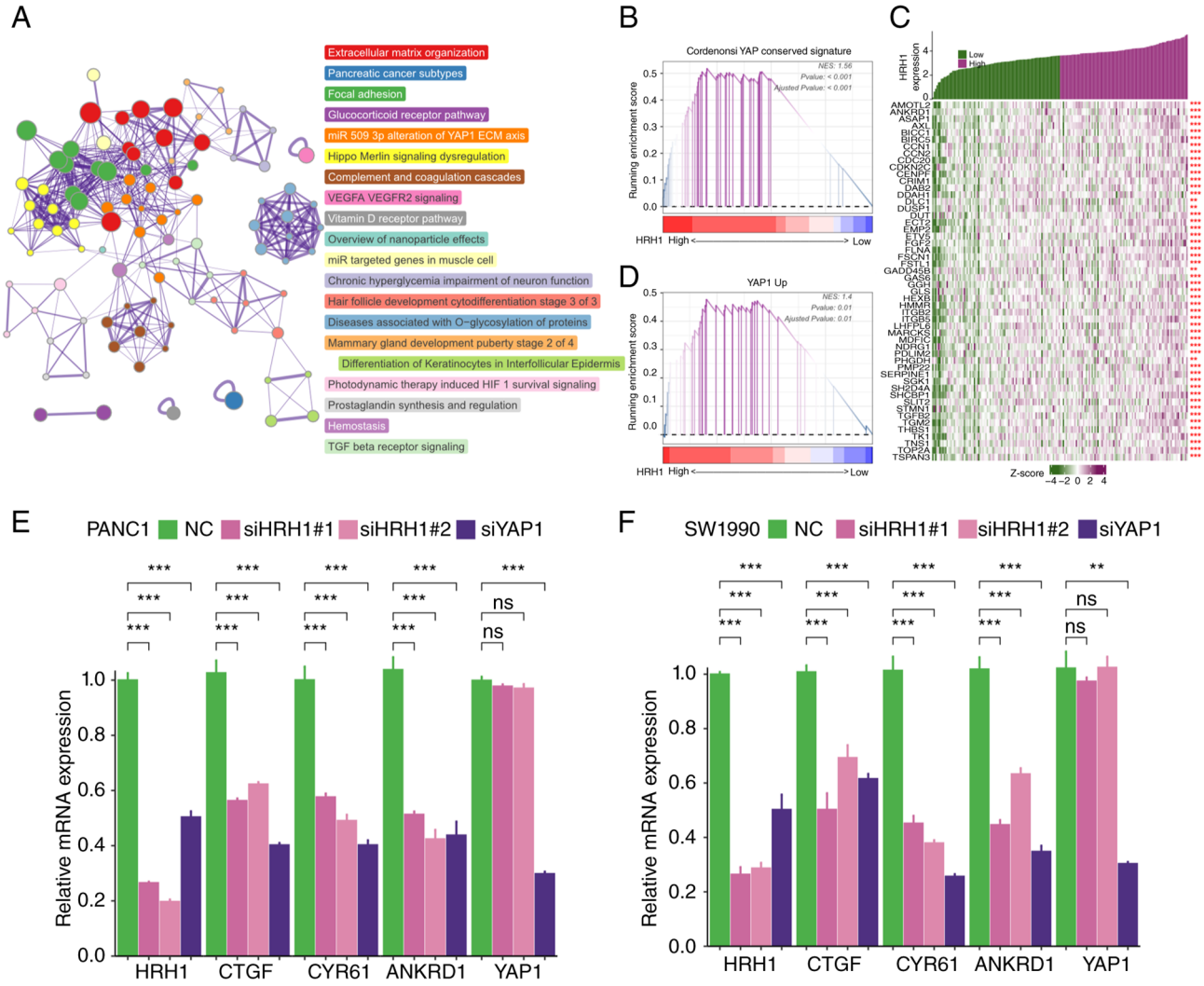

Figure 3. HRH1 is associated with YAP1 signaling. (A) Metascape enrichment analysis revealed that HRH1 is functionally associated with YAP1 signaling. The gene set was derived from differentially upregulated genes in the HRH1-high expression group within TCGA-PAAD cohort. Gene Set Enrichment Analysis further indicated a significant correlation between HRH1 and both the (B) 'Cordenosi YAP conserved signature' and the (D) 'YAP1 up signature'. (C) A heatmap illustrated HRH1 expression and the expression of multiple YAP1 pathway target genes. Based on HRH1 expression levels, TCGA PDAC groups were categorized into two groups to compare the expression of YAP1-targeted genes (***P<0.001). Expression changes of HRH1, CTGF, CYR61, ANKRD1 and YAP1 were assessed following knockdown of HRH1 and YAP1. The knockdown groups were compared with the non-targeting control in (E) PANC-1 and (F) SW1990 cells. Statistical significance was assessed by one-way ANOVA followed by Dunnett's post hoc test (***P<0.001, **P<0.01; ns, Not Significant). si, small interfering; NC, negative control.

in pancreatic cancer, the present study employed 101 distinct machine learning algorithms to construct prognostic models based on HRH1, YAP1 and YAP1 downstream genes associated with HRH1 expression (listed in Fig. 3D). A prognostic model was first constructed based on TCGA-PAAD training cohort, and individual risk scores were then generated for patients in both TCGA-PAAD and ICGC-PACA-AU cohorts, with the latter serving as an independent validation set. Batch effects were removed across different datasets (Fig. S5). The C-index was employed as the main evaluation metric to determine the model's predictive performance, reflecting the likelihood of agreement between model predictions and actual observed outcomes. Among the 101 algorithms evaluated, 25 models were successfully constructed. In TCGA cohort, the mean C-index was 0.659 (SD=0.069), while in the ICGC cohort, the mean C-index was 0.683 (SD=0.08; Fig. 5A). Among these, the 'plsRcox' approach, which combines partial least squares regression with Cox regression, achieved optimal predictive performance, exhibiting a mean C-index of 0.713. The HRH1/YAP1 signaling-derived prognostic signature comprises eight genes. Risk scores were computed based on a weighted linear combination of expression levels from eight signature genes, defined as: risk score=(0.032 x HRH1) + (0.015 x YAP1) + (0.227 x ECT2) + (0.215 x ITGB5) + (0.207 x SHCBP1) + (0.108 x MAML2) + (0.032 x YWHAZ) + (0.147 x ITGA2). Analysis revealed that the risk score based on HRH1/YAP1 signaling emerged as an independent determinant of overall survival in pancreatic cancer patients, as shown by univariate and multivariate Cox regression (Fig. 5B and C).

To further validate the robustness of the model, two additional GEO datasets (GSE28735 and GSE183795), which were not used during model training, were employed as external validation sets. Higher risk scores were associated

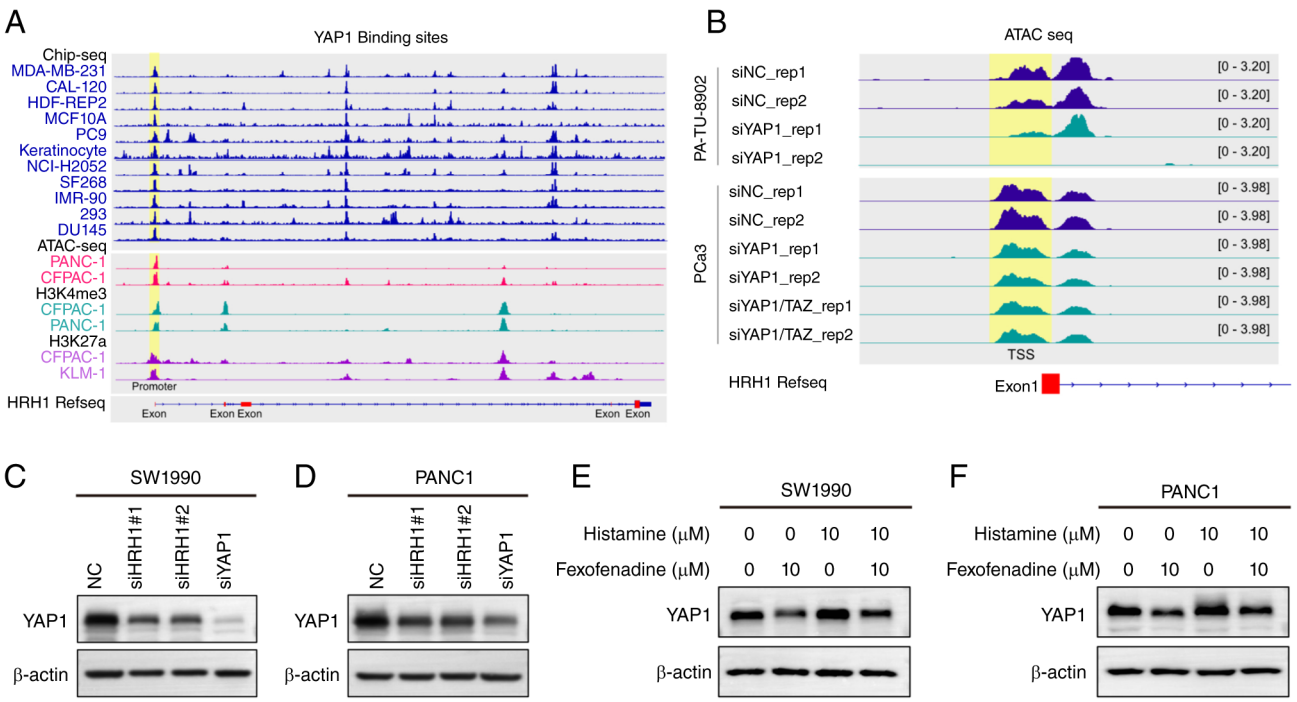

Figure 4. The reciprocal regulation between YAP1 and HRH1. (A) YAP1 binds to the promoter region of HRH1. The ChIP-seq data for H3K4me3, H3K27ac and YAP1, as well as ATAC-seq data, were obtained from the ChIP-Atlas database. (B) In PA-TU-8902 and PCa3 cells, knockdown of YAP1 and TAZ resulted in reduced chromatin accessibility at the HRH1 promoter region. ATAC-seq data for PA-TU-8902 and PCa3 were obtained from the ChIP-Atlas database. Knockdown of HRH1 and YAP1 led to a marked reduction in YAP1 protein levels in (C) SW199 and (D) PANC10 cells. The observed molecular weights of β-actin and YAP1 were ~42 and 75 kDa, respectively. Relative YAP1 expression levels, normalized to β-actin and the NC, are provided in Table SVIII. Treatment of (E) SW1990 and (F) PANC1 cells with fexofenadine and histamine resulted in altered expression of YAP1. Relative YAP1 expression levels, normalized to β-actin and the Control group, are provided in Table SIX. si, small interfering; NC, negative control.

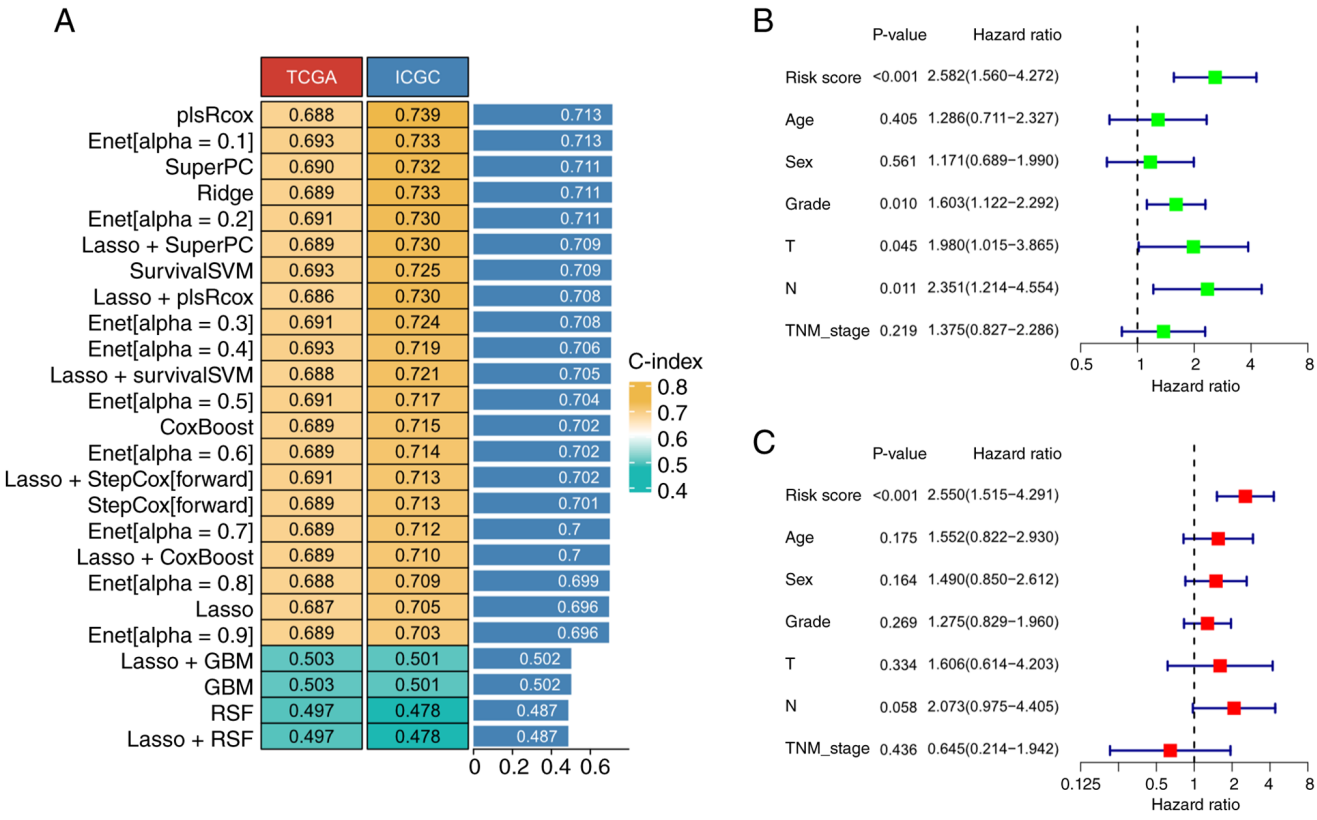

Figure 5. Construction of prognostic models using 113 distinct machine learning algorithms. (A) The top 25 prognostic models established through 103 distinct machine learning approaches. Model ranking was determined by the average C-index across both the training set (TCGA-PAAD) and the validation set (ICGC-PACA-AU). (B) Uni- and (C) multivariate Cox regression analyses were performed to evaluate the prognostic model derived from the 'plsRcox' algorithm within TCGA cohort. TCGA, The Cancer Genome Atlas.

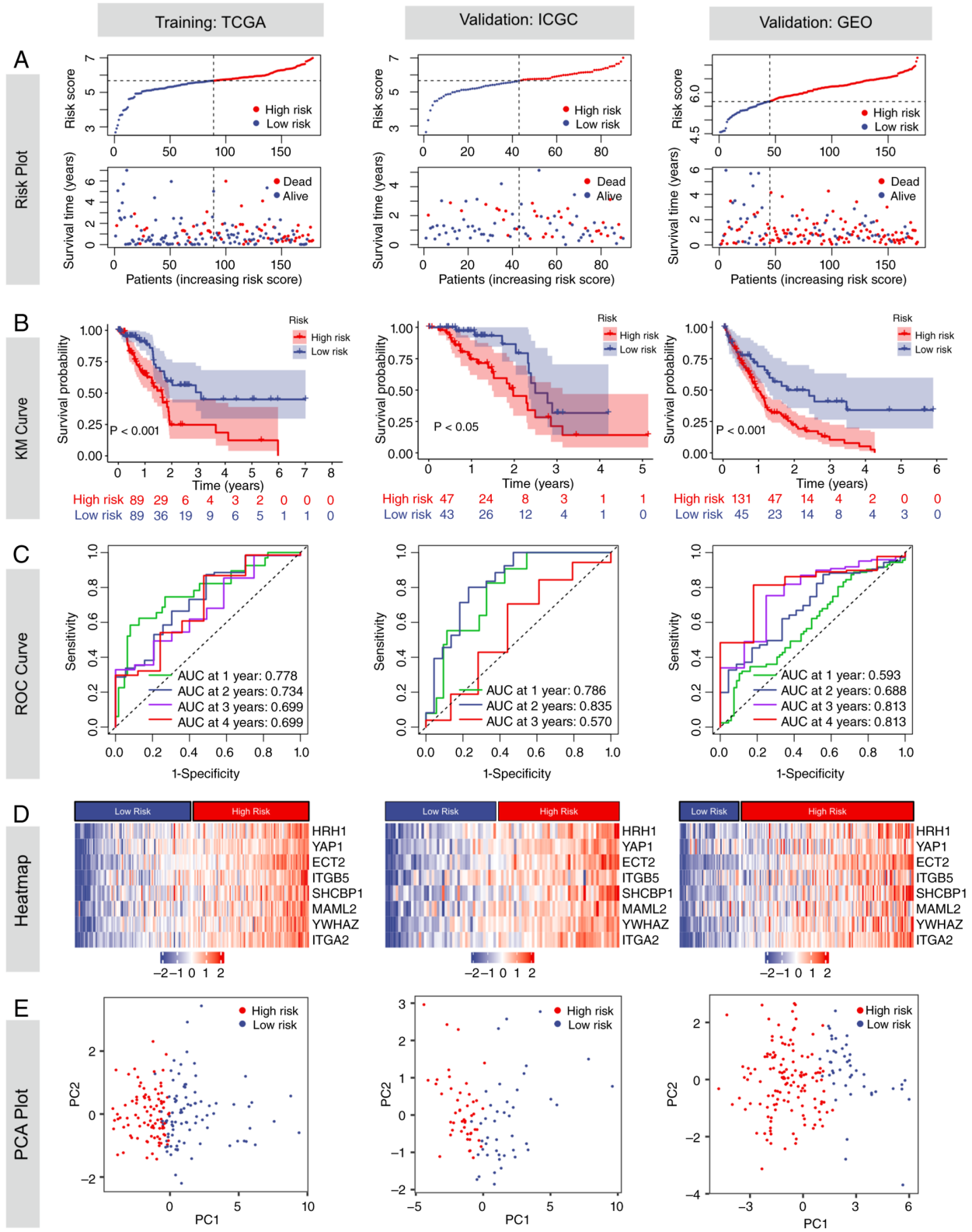

Figure 6. Prognostic value of the HRH1/YAP1 signaling axis-derived signature in TCGA, ICGC and GEO cohorts. (A) Risk score distribution plots demonstrating the correlation between elevated risk scores and mortality events. (B) Kaplan-Meier curves stratified by risk groups. (C) Time-dependent receiver operating characteristic curves assessing the model's predictive accuracy for 1-, 2-, 3- and 4-year survival. (D) Expression heatmaps of the eight signature genes incorporated in the risk model. (E) PCA visualizing the separation between high- and low-risk groups. PCA, principal component analysis; KM, Kaplan-Meier. TCGA, The Cancer Genome Atlas; ICGC, International Cancer Genome Consortium; GEO, Gene Expression Omnibus.

with increased mortality (Fig. 6A). Using the median risk score of 6.171 from TCGA-PAAD training cohort as the cut-off, both the training and validation sets were stratified into high- and low-risk groups. KM analysis revealed significantly worse survival in the high-risk group, with log-rank P<0.001 in TCGA-PAAD and GEO cohorts, and P<0.05 in

the ICGC-PACA-AU cohort (Fig. 6B). Time-dependent ROC analysis demonstrated that the AUC values for predicting 1-, 2-, 3- and 4-year survival were 0.778/0.734/0.699/0.699 in TCGA-PAAD, 0.786/0.835/0.570/NA in ICGC-PACA-AU and 0.593/0.688/0.813/0.813 in GEO, respectively (Fig. 6C). The time-dependent Brier scores for 1-, 2-, 3- and 4-year overall survival prediction were 0.143, 0.185, 0.190, and 0.182 in TCGA-PAAD cohort; 0.115, 0.185, 0.202, and 0.182 in the ICGC-PACA-AU cohort; and 0.242, 0.187, 0.128, and 0.100 in the GEO cohort, respectively. Lower Brier scores indicate improved calibration and predictive accuracy (Fig. S6). Heatmap analysis demonstrated a positive correlation between all model genes and the risk score (Fig. 6D). PCA analysis showed clear separation between high- and low-risk groups, with non-overlapping distributions in the scatter plot (Fig. 6E).

High-risk scores are associated with high TMB, chemoresistance and immunosuppression. Previous studies have reported that targeting HRH1 can enhance the sensitivity to ICIs by upregulating MHC-I expression in pancreatic cancer, while targeting YAP1 increases chemosensitivity to gemcitabine (62,63). Inspired by these findings, the present study further investigated the association between the HRH1/YAP1 signaling-related risk score and sensitivity to both chemotherapeutic agents and ICIs. As illustrated in Fig. 7A, high-risk patients demonstrated markedly elevated IC_{50} levels for standard chemotherapeutic agents used in PDAC treatment. These included gemcitabine, fluorouracil, SN-38 (the active derivative of irinotecan), and oxaliplatin, along with other commonly administered drugs such as platinum-based compounds, doxorubicin, mitomycin and vincristine. Further analysis revealed a higher mutation frequency of the pancreatic cancer driver gene KRAS in the high-risk group (85 vs. 44%), with similar trends observed for TP53 (78 vs. 44%), SMAD4 (26 vs. 16%) and CDKN2A (26 vs. 11%). The heightened chemoresistance and worse prognosis evident in high-risk patients may be partially attributable to mutations within these genes (Fig. 7B) (5,64).

Although TMB is generally associated with improved response to immunotherapy, with a typical cut-off for TMB-high defined as 10 muts/Mb (65-67). The present analysis revealed a positive correlation between the risk score and TMB. However, the majority of samples demonstrated a TMB below 4 muts/Mb. This suggests that these patients are unlikely to respond favorably to ICIs (Fig. 7D). The present analysis of the TME further revealed that a high risk score was associated with an enriched presence of immunosuppressive cells, including myeloid-derived suppressor cells (MDSCs), cancer-associated fibroblasts (CAFs), regulatory T cells (Tregs) and T helper 2 cells (Th2 cells) (Figs. 7C and S7). In contrast, this high-risk phenotype was characterized by a significant decrease in $CD8^+$ T cells. The TIDE algorithm, designed to forecast responses to ICI treatment, yielded elevated scores in the high-risk group (Fig. 7E). Elevated TIDE values are associated with a greater likelihood of unfavorable therapeutic outcomes. Therefore, although pancreatic cancer is generally considered an 'immune-cold' tumor with limited response to ICIs, the low-risk group benefiting from immunotherapy.

Discussion

PDAC has a 5-year survival rate of merely 13% and limited therapeutic advancements over the past four decades (2). Its recalcitrance stems from an immunosuppressive TME, early metastatic dissemination and rapid acquisition of chemoresistance. These factors collectively render conventional therapy ineffective for the majority of patients (68). It is increasingly recognized that tumors are not merely passive entities evading host control but are active 'hijackers' of systemic homeostasis (69). They achieve this by producing and releasing a wide array of neuroendocrine mediators, including classical neurotransmitters, biogenic amines (such as histamine) and hormones. These substances reprogram central regulatory axes and reset the body's physiological state to create an environment that favors tumor expansion. For instance, serotonin promotes the proliferation and progression of cholangiocarcinoma by upregulating tryptophan hydroxylase 1 (TPH1) expression and dysregulating its metabolic pathway in tumor cells (70). Targeting serotonin synthesis with telotristat ethyl or blocking specific 5-hydroxytryptamine (5-HT) receptors represents a promising therapeutic strategy for advanced cholangiocarcinoma. Similarly, melanoma promotes the secretion of pituitary hormones through autocrine and paracrine pathways, and these hormones in turn drive melanoma cell proliferation, invasion and malignant progression via activating downstream signaling cascades (71). For instance, cholangiocarcinoma cells actively usurp the physiological serotonin metabolic pathway (70). They upregulate TPH1 (the rate-limiting enzyme for serotonin synthesis) and downregulate MAO-A (the serotonin-degrading enzyme), leading to pathological overproduction of serotonin. Instead of serotonin acting as a homeostatic regulator, cholangiocarcinoma cells express all 5-HT receptor subtypes to establish an autocrine loop that drives cell proliferation and progression, thereby rewiring normal physiological regulation to create a pro-TME. Melanoma cells secrete thyrotropin-releasing hormone and thyroid-stimulating hormone (TSH) via autocrine and paracrine pathways (71). These hormones act through functionally expressed melanocortin-1 receptor and TSH receptors, respectively, to drive malignant progression (72). Activation of these receptors initiates cAMP signaling and MAPK pathway cascades, while crosstalk with the PI3K/Akt pathway potentiates melanoma proliferation, invasion and transformation. The present study identified HRH1, a G protein-coupled receptor, as a key regulator of PDAC progression, operating through a previously unrecognized positive regulatory loop with the transcriptional coactivator YAP1. These findings not only illuminate a novel signaling axis driving PDAC pathogenesis but also provide a rationale for repurposing existing HRH1 antagonists (fexofenadine) as targeted therapies, alongside a prognostic model to guide patient stratification.

GPCRs represent a major drug target class, with ~34% of all currently marketed Food and Drug Administration-approved drugs acting through direct or indirect modulation of GPCR activity (8). GPCRs control Hippo signaling and YAP1 transactivation in a G protein-dependent manner (73). Ligand-stimulated GPCRs coupled to $G\alpha_{12}/_{13}$, $G\alpha q/_{11}$ or $G\alpha i/o$ suppress LATS1/2 kinase activity, reduce YAP1 phosphorylation and drive its nuclear entry to boost TEAD-mediated

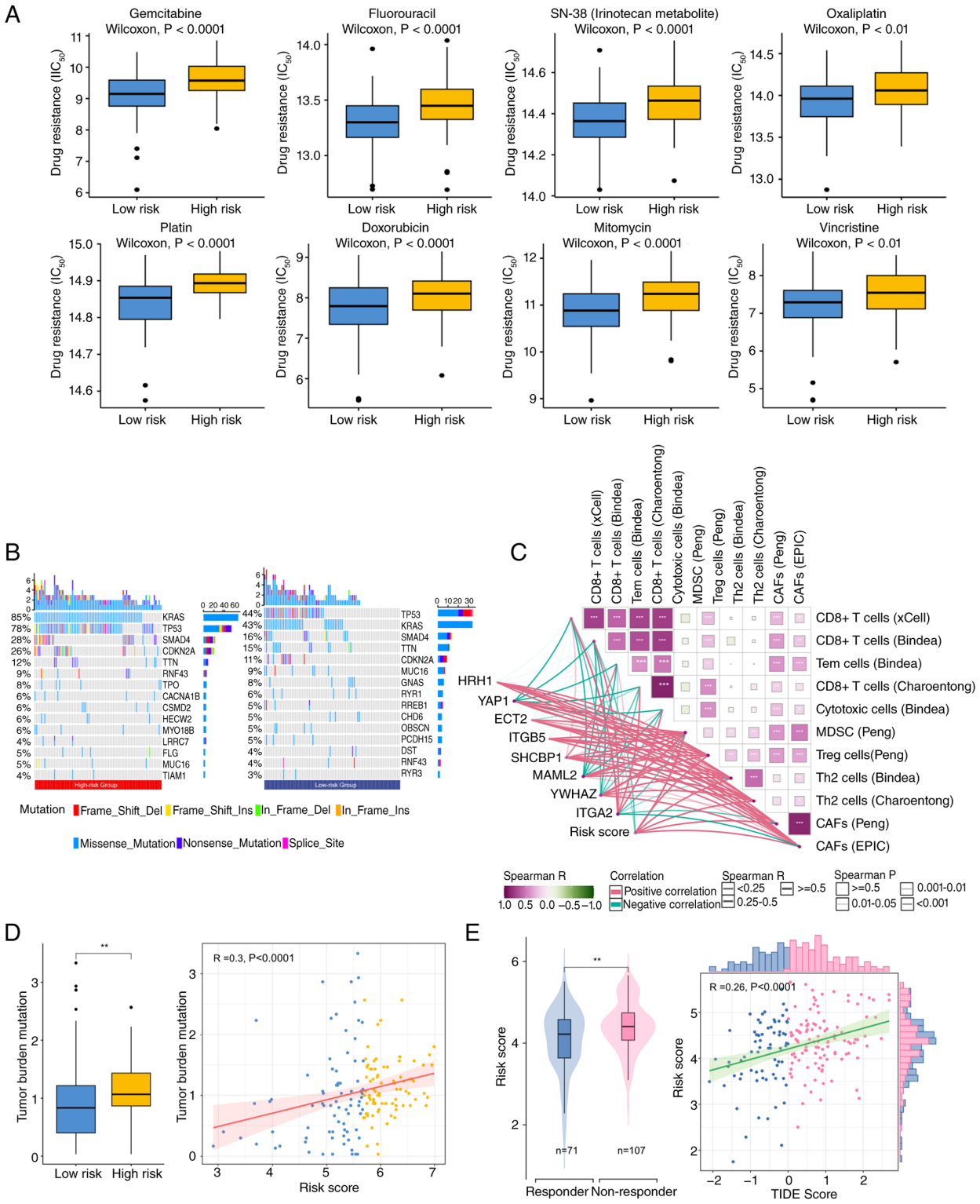

Figure 7. Chemotherapy resistance, TMB, tumor-infiltrating immune cells and ICI sensitivity in TCGA-PAAD cohort. (A) Comparison of chemotherapy resistance between high- and low-risk patients. Chemoresistance was predicted using the 'oncoPredict' R package. Statistical comparisons were performed using the Wilcoxon rank-sum test. (B) Oncoplots depicting the top 15 mutated genes and their mutation frequencies in the high- and low-risk groups. (C) Correlation matrix illustrating the association between the abundance of tumor-infiltrating immune cells and the eight-gene signature. Correlations were examined using Spearman's rank method. (D) Correlation between risk score and TMB. The data were analyzed using Spearman's rank correlation and Wilcoxon rank-sum tests (**P<0.01). (E) Evaluation of ICI treatment efficacy using the TIDE computational framework. A higher TIDE score indicates poorer response to immune checkpoint inhibitor therapy. **P<0.01). TMB, tumor mutational burden; ICI, immune checkpoint inhibitor.

transcription. By contrast, Gαs-coupled GPCRs trigger PKA signaling that enhances LATS1/2-dependent YAP1 phosphorylation, sequestering YAP1 in the cytoplasm and silencing its transcriptional function. The present study integrated analysis of multiple cohorts established that HRH1 is substantially upregulated in PDAC. This upregulation was evident at both

bulk and single-cell resolution and was specifically enriched in malignant cells compared with their normal counterparts. Elevated HRH1 expression levels were identified as an independent predictor of shortened overall survival among patients in TCGA-PAAD cohort. HRH1, initially recognized as a therapeutic target for managing allergic inflammatory responses, has more recently been associated with the advancement of multiple cancer types. HRH1 is highly expressed in oral squamous cell carcinoma and is markedly associated with lymph node metastasis and poor prognosis (74). HRH1 promotes the progression of oral squamous cell carcinoma by triggering the epithelial-mesenchymal transition process through activation of ADAM9-mediated TGF-β signaling and upregulation of Snail family transcription factors (74). Activation of HRH1 signaling enhances development of intestinal tumors *in vivo* and stimulated the proliferation of intestinal epithelial cells derived from colorectal cancer (75). The radiosensitizing effect mediated by HRH1 inhibition with loratadine was corroborated in multiple cancer cell models, including colon cancer, glioblastoma and prostate cancer (76). Hrh1 was predominantly the only histamine receptor subtype expressed among the other three Hrhs (Hrh2, Hrh3 and Hrh4) in Kras-LSL$^{G12D/+}$; Trp53$^{fl/fl}$; Ptf1a-Cre$^{+/-}$ PDAC cell lines (77). PANC-1 cells utilize autocrine and paracrine histamine signaling through HRH1 to promote proliferation via nerve growth factor upregulation, an effect reversible by the HRH1 antagonist pyrilamine. Consistent with prior observations, the CCK-8 assay results of the present study revealed that knockdown of HRH1 markedly suppressed the proliferation of PDAC cells (77). MR analysis reinforced a potential causal relationship between HRH1 inhibition and reduced PDAC risk. Similarly, in patients with breast cancer and melanoma, the use of antihistamine drugs such as desloratadine and loratadine was associated with prolonged overall survival (78,79). Therefore, HRH1 has emerged as a potential therapeutic target in multiple cancer types due to its role in promoting tumor cell proliferation and metastasis.

HRH1 primarily couples to Gαq/11 proteins, which activate phospholipase C (80). The activation of this pathway initiates the generation of second messengers, inositol trisphosphate and diacylglycerol, leading to a rapid increase in intracellular Ca^{2+} levels. This Ca^{2+} surge promotes the activation of protein kinase C, which in turn stimulates the Rho/ROCK pathway and induces F-actin polymerization. The resulting cytoskeletal remodeling suppresses LATS1/2 kinase activity, thereby modulating multiple pro-tumorigenic signaling cascades (6). In parallel, Ca^{2+} binds to calmodulin (CaM), forming a Ca^{2+}/CaM complex. This complex enhances the inhibitory phosphorylation of YAP by LATS1, thereby activating the Hippo pathway and ultimately restraining YAP-driven transcriptional activity (81). Importantly, as a GPCR, HRH1 is positioned to transduce extracellular histamine signals into intracellular responses that directly impinge on the Hippo/YAP1 pathway. The present study reveals that HRH1 operates as a key upstream regulator of YAP1, forming a positive feedback loop that amplifies oncogenic signaling. The downstream mechanisms mediated by HRH1 in PDAC remain poorly understood. While data of the present study demonstrate that HRH1 inhibition reduces YAP1 protein levels without altering its transcript abundance, the precise post-translational mechanism remains to be fully elucidated. Based on established GPCR-Hippo crosstalk, we hypothesize that HRH1 signaling, potentially through Gαq-mediated activation of Rho/ROCK/F-actin, suppresses LATS1/2 kinase activity. This suppression may reduce YAP1 phosphorylation at Ser127, a modification that is essential for recognition by the β-TrCP E3 ubiquitin ligase complex and subsequent β-TrCP-mediated ubiquitination and degradation (61,82). Future investigations should prioritize protein stability assays using cycloheximide and MG132 treatments, subcellular fractionation studies and phospho-specific immunoblotting of YAP1 to validate the proposed mechanism.

Conversely, YAP1 could enhance HRH1 transcription by binding to its promoter, as evidenced by ChIP-seq peaks, active histone marks (H3K4me3 and H3K27ac) and open chromatin (ATAC-seq) at the HRH1 locus. In addition, knockdown of HRH1 in human endothelial cells downregulated YAP1 target genes, such as CCN1 and CCN2, while silencing of YAP1 reduced HRH1 expression across multiple cancer cell lines. The present findings indicate that HRH1-YAP1 signaling is consistently observed across multiple human cancer cell types and is not restricted to pancreatic cancer cells. This feedback loop provides a molecular explanation for the strong association between HRH1 expression and YAP1 target genes (CYR61, CTGF and ANKRD1) in PDAC patient data. A similar regulatory mechanism has been observed in other malignancies. For instance, CXCR7 activates YAP through Gαq/11 and Rho GTPase signaling, while YAP transcriptionally upregulates CXCR7 expression, establishing a positive feedback loop that promotes gastric cancer progression (83). Therefore, to the best of our knowledge, the present study demonstrates for the first time that HRH1 and YAP1 form a positive regulatory loop that cooperatively drives the progression of pancreatic cancer.

KRAS mutations represent the most prevalent genetic alterations in PDAC. The predominant mutated variants included G12D (36.2%), G12V (26.2%), G12R (14.3%) and Q61 (5.3%), while the remaining 15.5% were identified as KRAS wild-type (84). Mutant Kras constitutively activates multiple downstream effector pathways, leading to pancreatic cancer initiation, progression, chemotherapy resistance and immune suppression, including the RAF-MEK-ERK (MAPK) cascade and the PI3K-AKT-mTOR axis (84,85). The approval of the first G12C inhibitor, sotorasib, in 2021 represented a major therapeutic advance (86). In parallel, the ongoing clinical investigation of G12D inhibitors and pan-RAS inhibitors heralds the advent of a new era in precision medicine for PDAC (86). The Hippo-YAP1 pathway has emerged as a central mediator of PDAC progression, enabling tumors to bypass oncogenic KRAS dependency and resist KRAS-targeted therapies (13,87). Moreover, prior evidence indicates that YAP1 confers resistance to gemcitabine-based chemotherapy regimens (88). Although KRAS does not directly interact with core Hippo components or YAP1, their functional crosstalk is mediated by specific scaffold proteins that establish precise molecular linkages (89-91). For instance, RASSF5 directly binds GTP-bound KRAS via its RA domain and simultaneously recruits MST1 through its SARAH motif. This ternary complex promotes cytoplasmic retention of YAP1, thereby inhibiting its nuclear translocation and transcriptional activity, providing a defined mechanism by which activated KRAS engages the Hippo pathway (89). In parallel, KSR1 serves as a dual-function scaffold that dynamically coordinates both pathways: Under basal conditions, it constitutively associates with MST1, LATS1 and YAP1 to

enhance YAP1-driven transcription; upon EGF stimulation or KRAS activation, KSR1 disengages from Hippo components and instead nucleates Raf-MEK-ERK complexes to potentiate MAPK signaling (90). In the present study, the high-risk subgroup exhibiting elevated YAP1 expression demonstrated a significantly higher frequency of KRAS mutations. Chemoresistance analysis further revealed that high HRH1 expression is associated with resistance to gemcitabine, agents within the FOLFIRINOX regimen and multiple other cytotoxic compounds. Disruption of the HRH1-YAP1 regulatory axis may therefore address a key therapeutic challenge by mitigating the functional redundancy between KRAS and YAP1, which currently limits the efficacy of both targeted therapies and conventional chemotherapy. Repurposing fexofenadine, an antihistamine drug characterized by a favorable safety profile, may circumvent the protracted development timelines associated with novel therapeutic agents, thereby providing a viable and expeditious route for clinical translation.

Beyond identifying a novel signaling axis, the present study translated these findings into a clinically actionable tool: A prognostic model based on HRH1, YAP1 and downstream targets (ECT2, ITGB5, SHCBP1, MAML2, YWHAZ and ITGA2). To improve risk stratification for high-risk patients, the present study developed a model by systematically assessing 113 algorithms in TCGA cohort, with external validation in ICGC and GEO datasets. This model provides a robust tool for clinical risk stratification, demonstrating superior prognostic accuracy over conventional TNM staging. Notably, high-risk scores were correlated with resistance to both chemotherapy and immunotherapy, a finding consistent with the established oncogenic role of YAP1 (88,92). Elevated TMB (10 muts/Mb) typically correlates with enhanced efficacy of immunotherapeutic interventions, owing to the increased production of immunogenic neoantigens that facilitate improved immune system recognition and elimination (54-56). PDAC is generally characterized by a low TMB (typically ranging from 1 to 4 mutations/megabase), which contributes to the limited efficacy of immunotherapy in this malignancy (93). Although the high-risk subgroup demonstrates relatively elevated TMB and may exhibit increased sensitivity to ICIs against PD-1 and PD-L1, the therapeutic outcome is also critically influenced by the cellular composition of the TME. Studies have demonstrated that YAP1 acts as a transcriptional driver of multiple cytokines, which subsequently promote the differentiation and accumulation of MDSCs, CAFs and Tregs (94-97). This contributes to the establishment of a robust immune-cold TME in PDAC. In the present study, high-risk patients exhibited elevated YAP1 expression, and analysis of the TME revealed that the risk score was significantly positively associated with the abundance of CAFs, MDSCs, Th2 cells and Tregs. Moreover, activation of HRH1 drives macrophage polarization toward an M2-like phenotype, leading to impaired T cell function (98). By contrast, blocking HRH1 elevates MHC-I levels in PDAC via the cholesterol biosynthesis pathway (62). Dual inhibition of HRH1 and PD-1 improved CD8+ T cell infiltration and cytotoxicity, effectively countering resistance to ICI therapy. These findings suggest that pharmacological antagonism of HRH1 may enhance antitumor immunity and potentiate the efficacy of immunotherapy.

While the present study provides a foundation for targeting HRH1 in PDAC, several limitations warrant consideration. First, while the prognostic model exhibited strong predictive accuracy across both the training cohort and two independent validation sets, its clinical utility requires further validation in prospective studies. Second, although the MR analysis indicates a potential causal link, it depends on SNPs as proxies for fexofenadine exposure. Therefore, prospective clinical studies are necessary to conclusively confirm its effectiveness. Third, the present study only demonstrates that HRH1 promotes YAP1 protein stabilization, without further elucidating the specific regulatory pathways involved. Future studies should delineate the mechanisms by which HRH1 regulates YAP1 stability and determine whether HRH1-mediated YAP1 activation depends on KRAS mutation status. Fourth, while integrative analysis of public ChIP-seq and ATAC-seq datasets strongly supports YAP1 occupancy at the HRH1 promoter, direct experimental validation in PDAC cells has not been performed and remains a limitation of the present study. Luciferase reporter assays and ChIP-qPCR experiments are currently planned as part of the future work. Fifth, the present analysis of HRH1 expression is based on transcriptomic data from multiple public databases and patient cohorts. HRH1 protein expression was not validated across different pancreatic cancer cell lines or in clinical tumor samples. However, a recent study reported elevated HRH1 protein levels in pancreatic cancer tissues compared to adjacent non-tumor tissues (62). Future studies should prioritize experimental validation of HRH1 at the protein level and further investigate its functional role in modulating the crosstalk between KRAS and the Hippo/YAP1 signaling pathway, which may reveal novel therapeutic vulnerabilities in PDAC. Additionally, the present study did not consider the contribution of exogenous histamine from immune cells (such as mast cells) in the TME. This gap warrants further investigation, given that stromal-derived histamine may serve as an endogenous HRH1 agonist and amplify the HRH1-YAP1 feedback loop.

In summary, the present study identified HRH1 as a key driver of PDAC progression, functioning via a positive feedback loop with YAP1 to amplify oncogenic signaling, promote chemoresistance and potentiate immunosuppression. The HRH1/YAP1 prognostic model offers a powerful tool for patient stratification. Collectively, these findings provide a novel therapeutic strategy for PDAC by leveraging the druggability of HRH1 to disrupt a key oncogenic signaling axis.

Acknowledgements

Not applicable.

Funding

This work was supported by the Scientific Research Startup Fund of Chengdu Third People's Hospital (Grant no. CSY-YN-04-2024-008).

Availability of data and materials

The data generated in the present study may be requested from the corresponding author.

Authors' contributions

JC and JW conceived and designed the study and co-wrote the original draft of the manuscript. JC performed bioinformatic analyses, data curation and *in vitro* experiments (including CCK-8 assay, western blotting, RT-qPCR and ChIP-qPCR). JW was responsible for statistical analysis. Both JC and JW confirm the authenticity of all the raw data. Both authors read and approved the final version of the manuscript.

Ethics approval and consent to participate

Not applicable.

Patient consent for publication

Not applicable.

Competing interests

The authors declare that they have no competing interests.

Use of artificial intelligence tools

During the preparation of this work, artificial intelligence tools were used to improve the readability and language of the manuscript, and subsequently, the authors revised and edited the content produced by the artificial intelligence tools as necessary, taking full responsibility for the ultimate content of the present manuscript.

References

1. Mackay TM, Latenstein AEJ, Augustinus S, van der Geest LG, Bogte A, Bonsing BA, Cirkel GA, Hol L, Busch OR, den Dulk M, *et al*: Implementation of best practices in pancreatic cancer care in the netherlands: A Stepped-wedge randomized clinical trial. JAMA Surg 159: 429-437, 2024.
2. Siegel RL, Kratzer TB, Giaquinto AN, Sung H and Jemal A: Cancer statistics, 2025. CA Cancer J Clin 75: 10-45, 2025.
3. Rahib L, Smith BD, Aizenberg R, Rosenzweig AB, Fleshman JM and Matrisian LM: Projecting cancer incidence and deaths to 2030: The unexpected burden of thyroid, liver, and pancreas cancers in the United States. Cancer Res 74: 2913-2921, 2014.
4. Zhu Y, Fang S, Fan B, Xu K, Xu L, Wang L, Zhu L, Chen C, Wu R, Ni J and Wang J: Cancer-associated fibroblasts reprogram cysteine metabolism to increase tumor resistance to ferroptosis in pancreatic cancer. Theranostics 14: 1683-1700, 2024.
5. Stoop TF, Javed AA, Oba A, Koerkamp BG, Seufferlein T, Wilmink JW and Besselink MG: Pancreatic cancer. Lancet 405: 1182-1202, 2025.
6. Ahn S and Kaipparettu BA: G-protein coupled receptors in metabolic reprogramming and cancer. Pharmacol Ther 270: 108849, 2025.
7. Krumm BE and Roth BL: Intracellular GPCR modulators enable precision pharmacology. NPJ Drug Discov 2: 8, 2025.
8. Arang N and Gutkind JS: G Protein-Coupled receptors and heterotrimeric G proteins as cancer drivers. FEBS Lett 594: 4201-4232, 2020.
9. Kim E, Riehl BD, Bouzid T, Yang R, Duan B, Donahue HJ and Lim JY: YAP mechanotransduction under cyclic mechanical stretch loading for mesenchymal stem cell osteogenesis is regulated by ROCK. Front Bioeng Biotechnol 11: 1306002, 2024.
10. Zhou T, Li X, Liu J and Hao J: The Hippo/YAP signaling pathway: The driver of cancer metastasis. Cancer Biol Med 20: 483-489, 2023.
11. Yan H, Yu CC, Fine SA, Youssof AL, Yang YR, Yan J, Karg DC, Cheung EC, Friedman RA, Ying H, *et al*: Loss of the Wild-type KRAS allele promotes pancreatic cancer progression through functional activation of YAP1. Oncogene 40: 6759-6771, 2021.
12. Kapoor A, Yao W, Ying H, Hua S, Liewen A, Wang Q, Zhong Y, Wu CJ, Sadanandam A, Hu B, *et al*: Yap1 activation enables bypass of oncogenic Kras addiction in pancreatic cancer. Cell 158: 185-197, 2014.
13. Gurreri E, Genovese G, Perelli L, Agostini A, Piro G, Carbone C and Tortora G: KRAS-dependency in pancreatic ductal adenocarcinoma: Mechanisms of escaping in resistance to KRAS inhibitors and perspectives of therapy. Int J Mol Sci 24: 9313, 2023.
14. Yang S, Tang W, Azizian A, Gaedcke J, Ströbel P, Wang L, Cawley H, Ohara Y, Valenzuela P, Zhang L, *et al*: Dysregulation of HNF1B/Clusterin axis enhances disease progression in a highly aggressive subset of pancreatic cancer patients. Carcinogenesis 43: 1198-1210, 2022.
15. Zhang G, Schetter A, He P, Funamizu N, Gaedcke J, Ghadimi BM, Ried T, Hassan R, Yfantis HG, Lee DH, *et al*: DPEP1 inhibits tumor cell invasiveness, enhances chemosensitivity and predicts clinical outcome in pancreatic ductal adenocarcinoma. PLoS One 7: e31507, 2012.
16. Lim SB: A microarray meta-dataset of pancreatic cancer. Version 1. ArrayExpress [dataset]. 2019. Available from: https://www.ebi.ac.uk/biostudies/studies/E-MTAB-6690.
17. Iwatate Y, Yokota H, Hoshino I, Ishige F, Kuwayama N, Itami M, Mori Y, Chiba S, Arimitsu H, Yanagibashi H, *et al*: Machine learning with imaging features to predict the expression of ITGAV, which is a poor prognostic factor derived from transcriptome analysis in pancreatic cancer. Int J Oncol 60: 60, 2022.
18. Pei H, Li L, Fridley BL, Jenkins GD, Kalari KR, Lingle W, Petersen G, Lou Z and Wang L: FKBP51 affects cancer cell response to chemotherapy by negatively regulating akt. Cancer Cell 16: 259-266, 2009.
19. Klett H, Fuellgraf H, Levit-Zerdoun E, Hussung S, Kowar S, Küsters S, Bronsert P, Werner M, Wittel U, Fritsch R, *et al*: Identification and validation of a diagnostic and prognostic Multi-Gene biomarker panel for pancreatic ductal adenocarcinoma. Front Genet 9: 108, 2018.
20. Idichi T, Seki N, Kurahara H, Yonemori K, Osako Y, Arai T, Okato A, Kita Y, Arigami T, Mataki Y, *et al*: Regulation of actin-binding protein ANLN by antitumor miR-217 inhibits cancer cell aggressiveness in pancreatic ductal adenocarcinoma. Oncotarget 8: 53180-53193, 2017.
21. Yang S, He P, Wang J, Schetter A, Tang W, Funamizu N, Yanaga K, Uwagawa T, Satoskar AR, Gaedcke J, *et al*: A novel MIF signaling pathway drives the malignant character of pancreatic cancer by targeting NR3C2. Cancer Res 76: 3838-3850, 2016.
22. Coggins GE, Farrel A, Rathi KS, Hayes CM, Scolaro L, Rokita JL and Maris JM: YAP1 mediates resistance to MEK1/2 inhibition in neuroblastomas with hyperactivated RAS signaling. Cancer Res 79: 6204-6214, 2019.
23. Enzo E, Santinon G, Pocaterra A, Aragona M, Bresolin S, Forcato M, Grifoni D, Perssion A, Zanconato F, Guzzo G, *et al*: Aerobic glycolysis tunes YAP/TAZ transcriptional activity. EMBO J 34: 1349-1370, 2015.
24. Weiler SME, Lutz T, Bissinger M, Sticht C, Knaub M, Gretz N, Schirmacher P and Breuhahn K: TAZ target gene ITGAV regulates invasion and feeds back positively on YAP and TAZ in liver cancer cells. Cancer Lett 473: 164-175, 2020.
25. Yang WH, Lin CC, Wu J, Chao PY, Chen K, Chen PH and Chi JT: The Hippo pathway effector YAP promotes ferroptosis via the E3 ligase SKP2. Mol Cancer Res 19: 1005-1014, 2021.
26. Chen J, Liu Z, Wu Z, Li W and Tan X: Identification of a chemoresistance-related prognostic gene signature by comprehensive analysis and experimental validation in pancreatic cancer. Front Oncol 13: 1132424, 2023.
27. Zhang Z, Wu HX, Lin WH, Wang ZX, Yang LP, Zeng ZL and Luo HY: EPHA7 mutation as a predictive biomarker for immune checkpoint inhibitors in multiple cancers. BMC Med 19: 26, 2021.
28. Chalmers ZR, Connelly CF, Fabrizio D, Gay L, Ali SM, Ennis R, Schrock A, Campbell B, Shlien A, Chmielecki J, *et al*: Analysis of 100,000 human cancer genomes reveals the landscape of tumor mutational burden. Genome Med 9: 34, 2017.
29. Dupain C, Gutman T, Girard E, Kamoun C, Marret G, Castel-Ajgal Z, Sablin MP, Neuzillet C, Borcoman E, Hescot S, *et al*: Tumor mutational burden assessment and standardized bioinformatics approach using custom NGS panels in clinical routine. BMC Biol 22: 43, 2024.
30. Qu S, Liu Z, Wang B, Li X, Li Z, Gai Y, Sun Y, Zhang Q, Sun Y, Pan W, *et al*: OTUD4 regulates pancreatic cancer progression via Hippo/YAP axis. Neoplasia 73: 101285, 2026.

31. Cherubini A, Rusconi F, Piras R, Wächtershäuser KN, Dossena M, Barilani M, Mei C, Hof L, Sordi V, Pampaloni F, *et al*: Exploring human pancreatic organoid modelling through single-cell RNA sequencing analysis. Commun Biol 7: 1527, 2024.
32. Ewers KM, Patil S, Kopp W, Thomale J, Quilitz T, Magerhans A, Wang X, Hessmann E and Dobbelstein M: HSP90 inhibition synergizes with cisplatin to eliminate Basal-like pancreatic ductal adenocarcinoma cells. Cancers (Basel) 13: 6163, 2021.
33. Lau AN, Li Z, Danai LV, Westermark AM, Darnell AM, Ferreira R, Gocheva V, Sivanand S, Lien EC, Sapp KM, *et al*: Dissecting cell-type-specific metabolism in pancreatic ductal adenocarcinoma. Elife 9: e56782, 2020.
34. Figueroa AL, Figueiredo H, Rebuffat SA, Vieira E and Gomis R: Taurine treatment modulates circadian rhythms in mice fed A high fat diet. Sci Rep 6: 36801, 2016.
35. Pozza ED, Dando I, Biondani G, Brandi J, Costanzo C, Zoratti E, Fassan M, Boschi F, Melisi D, Cecconi D, *et al*: Pancreatic ductal adenocarcinoma cell lines display a plastic ability to bi-directionally convert into cancer stem cells. Int J Oncol 46: 1099-1108, 2014.
36. Chaqour B: Molecular control of vascular development by the matricellular proteins CCN1 (Cyr61) and CCN2 (CTGF). Trends Dev Biol 7: 59-72, 2013.
37. Livak KJ and Schmittgen TD: Analysis of relative gene expression data using real-time quantitative PCR and the 2(-Delta Delta C(T)) method. Methods 25: 402-408, 2001.
38. Zu F, Chen H, Liu Q, Zang H, Li Z and Tan X: Syntenin regulated by miR-216b promotes cancer progression in pancreatic cancer. Front Oncol 12: 790788, 2022.
39. Gao D, Vela I, Sboner A, Iaquinta PJ, Karthaus WR, Gopalan A, Dowling C, Wanjala JN, Undvall EA, Arora VK, *et al*: Organoid cultures derived from patients with advanced prostate cancer. Cell 159: 176-187, 2014.
40. Mao N, Zhang Z, Lee YS, Choi D, Rivera AA, Li D, Lee C, Haywood S, Chen X, Chang Q, *et al*: Defining the therapeutic selective dependencies for distinct subtypes of PI3K pathway-altered prostate cancers. Nat Commun 12: 5053, 2021.
41. Wu T, Hu E, Xu S, Chen M, Guo P, Dai Z, Feng T, Zhou L, Tang W, Zhan L, *et al*: clusterProfiler 4.0: A universal enrichment tool for interpreting omics data. Innovation (Camb) 2: 100141, 2021.
42. Maeser D, Gruener RF and Huang RS: oncoPredict: An R package for predicting in vivo or cancer patient drug response and biomarkers from cell line screening data. Brief Bioinform 22: bbab260, 2021.
43. Zeng D, Fang Y, Qiu W, Luo P, Wang S, Shen R, Gu W, Huang X, Mao Q, Wang G, *et al*: Enhancing immuno-oncology investigations through multidimensional decoding of tumor microenvironment with IOBR 2.0. Cell Rep Methods 4: 100910, 2024.
44. Racle J, de Jonge K, Baumgaertner P, Speiser DE and Gfeller D: Simultaneous enumeration of cancer and immune cell types from bulk tumor gene expression data. Elife 6: e26476, 2017.
45. Aran D, Hu Z and Butte AJ: xCell: Digitally portraying the tissue cellular heterogeneity landscape. Genome Biol 18: 220, 2017.
46. Becht E, Giraldo NA, Lacroix L, Buttard B, Elarouci N, Petitprez F, Selves J, Laurent-Puig P, Sautès-Fridman C, Fridman WH and de Reyniès A: Estimating the population abundance of tissue-infiltrating immune and stromal cell populations using gene expression. Genome Biol 17: 218, 2016.
47. Finotello F, Mayer C, Plattner C, Laschober G, Rieder D, Hackl H, Krogsdam A, Loncova Z, Posch W, Wilflingseder D, *et al*: Molecular and pharmacological modulators of the tumor immune contexture revealed by deconvolution of RNA-seq data. Genome Med 11: 34, 2019.
48. Newman AM, Liu CL, Green MR, Gentles AJ, Feng W, Xu Y, Hoang CD, Diehn M and Alizadeh AA: Robust enumeration of cell subsets from tissue expression profiles. Nat Methods 12: 453-457, 2015.
49. Li T, Fu J, Zeng Z, Cohen D, Li J, Chen Q, Li B and Liu XS: TIMER2.0 for analysis of tumor-infiltrating immune cells. Nucleic Acids Res 48: W509-W514, 2020.
50. Jin Y, Wang Z, He D, Zhu Y, Chen X and Cao K: Identification of novel subtypes based on ssGSEA in immune-related prognostic signature for tongue squamous cell carcinoma. Cancer Med 10: 8693-8707, 2021.
51. Rooney MS, Shukla SA, Wu CJ, Getz G and Hacohen N: Molecular and genetic properties of tumors associated with local immune cytolytic activity. Cell 160: 48-61, 2015.
52. Charoentong P, Finotello F, Angelova M, Mayer C, Efremova M, Rieder D, Hackl H and Trajanoski Z: Pan-cancer immunogenomic analyses reveal Genotype-Immunophenotype relationships and predictors of response to checkpoint blockade. Cell Rep 18: 248-262, 2017.
53. Bindea G, Mlecnik B, Tosolini M, Kirilovsky A, Waldner M, Obenauf AC, Angell H, Fredriksen T, Lafontaine L, Berger A, *et al*: Spatiotemporal dynamics of intratumoral immune cells reveal the immune landscape in human cancer. Immunity 39: 782-795, 2013.
54. Danaher P, Warren S, Dennis L, D'Amico L, White A, Disis ML, Geller MA, Odunsi K, Beechem J and Fling SP: Gene expression markers of tumor infiltrating leukocytes. J Immunother Cancer 5: 18, 2017.
55. Jiang P, Gu S, Pan D, Fu J, Sahu A, Hu X, Li Z, Traugh N, Bu X, Li B, *et al*: Signatures of T cell dysfunction and exclusion predict cancer immunotherapy response. Nat Med 24: 1550-1558, 2018.
56. Shao G, Ma Y, Qu C, Gao R, Zhu C, Qu L, Liu K, Li N, Sun P and Cao J: Machine learning model based on the Neutrophil-to-Eosinophil ratio predicts the recurrence of hepatocellular carcinoma after surgery. J Hepatocell Carcinoma 11: 679-691, 2024.
57. Kordulewska N, Cieślińska A, Fiedorowicz E, Jarmołowska B and Kostyra E: Effect of the Fexofenadine on the expression of HRH-1 and HRH-4 receptor in peripheral blood mononuclear cell isolated from children with diagnosed allergy-in vitro study Short communication. J Pharm Pharm Sci 22: 93-97, 2019.
58. Zhou W, Lim A, Edderkaoui M, Osipov A, Wu H, Wang Q and Pandol S: Role of YAP signaling in regulation of programmed cell death and drug resistance in cancer. Int J Biol Sci 20: 15-28, 2024.
59. Creyghton MP, Cheng AW, Welstead GG, Kooistra T, Carey BW, Steine EJ, Hanna J, Lodato MA, Frampton GM, Sharp PA, *et al*: Histone H3K27ac separates active from poised enhancers and predicts developmental state. Proc Natl Acad Sci USA 107: 21931-21936, 2010.
60. Wang Z, Zang C, Rosenfeld JA, Schones DE, Barski A, Cuddapah S, Cui K, Roh TY, Peng W, Zhang MQ and Zhao K: Combinatorial patterns of histone acetylations and methylations in the human genome. Nat Genet 40: 897-903, 2008.
61. Babaahmadi-Rezaei H, Rezaei M, Ghaderi-Zefrehi H, Azizi M, Beheshti-Nasab H and Mehta JL: Reducing proteoglycan synthesis and NOX activity by ROCK inhibitors: Therapeutic targets in atherosclerosis. Endocr Metab Immune Disord Drug Targets 22: 1191-1200, 2022.
62. Zhong P, Nakata K, Oyama K, Higashijima N, Sagara A, Date S, Luo H, Hayashi M, Kubo A, Wu C, *et al*: Blockade of histamine receptor H1 augments immune checkpoint therapy by enhancing MHC-I expression in pancreatic cancer cells. J Exp Clin Cancer Res 43: 138, 2024.
63. Saito Y, Xiao Y, Yao J, Li Y, Liu W, Yuzhalin AE, Shyu YM, Li H, Yuan X, Li P, *et al*: Targeting a chemo-induced adaptive signaling circuit confers therapeutic vulnerabilities in pancreatic cancer. Cell Discov 10: 109, 2024.
64. Buscail L, Bournet B and Cordelier P: Role of oncogenic KRAS in the diagnosis, prognosis and treatment of pancreatic cancer. Nat Rev Gastro Hepat 17: 153-168, 2020.
65. Vega DM, Yee LM, McShane LM, Williams PM, Chen L, Vilimas T, Fabrizio D, Funari V, Newberg J, Bruce LK, *et al*: Aligning tumor mutational burden (TMB) quantification across diagnostic platforms: Phase II of the friends of cancer research TMB harmonization project. Ann Oncol 32: 1626-1636, 2021.
66. Krieger T, Pearson I, Bell J, Doherty J and Robbins P: Targeted literature review on use of tumor mutational burden status and programmed cell death ligand 1 expression to predict outcomes of checkpoint inhibitor treatment. Diagn Pathol 15: 6, 2020.
67. Meléndez B, Van Campenhout C, Rorive S, Remmelink M, Salmon I and D'Haene N: Methods of measurement for tumor mutational burden in tumor tissue. Transl Lung Cancer Res 7: 661-667, 2018.
68. Chung V, Mizrahi JD and Pant S: Novel therapies for pancreatic cancer. JCO Oncol Pract 21: 613-619, 2025.
69. Slominski RM, Raman C, Chen JY and Slominski AT: How cancer hijacks the body's homeostasis through the neuroendocrine system. Trends Neurosci 46: 263-275, 2023.
70. Balakrishna P, George S, Hatoum H and Mukherjee S: Serotonin pathway in cancer. Int J Mol Sci 22: 1268, 2021.
71. Chen YY, Liu LP, Zhou H, Zheng YW and Li YM: Recognition of melanocytes in Immuno-Neuroendocrinology and circadian rhythms: Beyond the conventional melanin synthesis. Cells 11: 2082, 2022.

72. Ulisse S, Baldini E, Pironi D, Gagliardi F, Tripodi D, Lauro A, Carbotta S, Tarroni D, D'Armiento M, Morrone A, *et al*: Is melanoma progression affected by thyroid diseases? Int J Mol Sci 23: 10036, 2022.
73. Luo J and Yu FX: GPCR-Hippo signaling in cancer. Cells 8: 426, 2019.
74. Ding YF, Ho KH, Lee WJ, Chen LH, Hsieh FK, Tung MC, Lin SH, Hsiao M, Yang SF, Yang YC and Chien MH: Cyclic increase in the histamine receptor H1-ADAM9-Snail/Slug axis as a potential therapeutic target for EMT-mediated progression of oral squamous cell carcinoma. Cell Death Dis 16: 191, 2025.
75. Shi Z, Fultz RS, Engevik MA, Gao C, Hall A, Major A, Mori-Akiyama Y and Versalovic J: Distinct roles of histamine H1- and H2-receptor signaling pathways in inflammation-associated colonic tumorigenesis. Am J Physiol Gastrointest Liver Physiol 316: G205-G216, 2019.
76. Soule BP, Simone NL, DeGraff WG, Choudhuri R, Cook JA and Mitchell JB: Loratadine dysregulates cell cycle progression and enhances the effect of radiation in human tumor cell lines. Radiat Oncol 5: 8, 2010.
77. Salmerón C, Tomás Bort E, Sriram K, Javadi-Paydar M, Smitham JE, Pham K, Grose RP, McCormick PJ, DiNardo A, Weitz J, *et al*: Histamine H1 Receptor: A potential therapeutic target for pancreatic ductal adenocarcinoma. J Pharmacol Exp Ther 392: 103573, 2025.
78. Fritz I, Wagner P, Bottai M, Eriksson H, Ingvar C, Krakowski I, Nielsen K and Olsson H: Desloratadine and loratadine use associated with improved melanoma survival. Allergy 75: 2096-2099, 2020.
79. Fritz I, Wagner P, Broberg P, Einefors R and Olsson H: Desloratadine and loratadine stand out among common H_1-antihistamines for association with improved breast cancer survival. Acta Oncol 59: 1103-1109, 2020.
80. Francis T, Graf A, Hodges K, Kennedy L, Hargrove L, Price M and Francis H: Histamine regulation of pancreatitis and pancreatic cancer: A review of recent findings. Hepatobil Surg Nutr 2: 216-226, 2013.
81. Thines L, Gorisse L, Li Z, Sayedyahossein S and Sacks DB: Calmodulin activates the Hippo signaling pathway by promoting LATS1 kinase-mediated inhibitory phosphorylation of the transcriptional coactivator YAP. J Biol Chem 298: 101839, 2022.
82. Vania V, Wang L, Tjakra M, Zhang T, Qiu J, Tan Y and Wang G: The interplay of signaling pathway in endothelial cells-matrix stiffness dependency with targeted-therapeutic drugs. Biochim Biophys Acta Mol Basis Dis 1866: 165645, 2020.
83. Wang T, Wang D, Sun Y, Zhuang T, Li X, Yang H, Zang Y, Liu Z, Yang P, Zhang C, *et al*: Regulation of the Hippo/YAP axis by CXCR7 in the tumorigenesis of gastric cancer. J Exp Clin Canc Res 42: 297, 2023.
84. Ebia MI, Blais EM, Cui Y, Petricoin EF III, Pishvaian M, Gaddam S, Gong J, Osipov A and Hendifar AE: Evaluating the effect of KRAS variants on survival outcomes and therapy response in pancreatic cancer. JCO Precis Oncol 9: e2400684, 2025.
85. Mahadevan KK, McAndrews KM, LeBleu VS, Yang S, Lyu H, Li B, Sockwell AM, Kirtley ML, Morse SJ, Moreno Diaz BA, *et al*: KRASG12D inhibition reprograms the microenvironment of early and advanced pancreatic cancer to promote FAS-mediated killing by CD8+ T cells. Cancer Cell 41: 1606-1620.e8, 2023.
86. Bannoura SF, Uddin MdH, Nagasaka M, Fazili F, Al-Hallak MN, Philip PA, El-Rayes B and Azmi AS: Targeting KRAS in pancreatic cancer: New drugs on the horizon. Cancer Metast Rev 40: 819-835, 2021.
87. Yang W, Zhang M, Zhang TX, Liu JH, Hao MW, Yan X, Gao H, Lei QY, Cui J and Zhou X: YAP/TAZ mediates resistance to KRAS inhibitors through inhibiting proapoptosis and activating the SLC7A5/mTOR axis. JCI Insight 9: e178535, 2024.
88. Zhou T, Xie Y, Hou X, Bai W, Li X, Liu Z, Man Q, Sun J, Fu D, Yan J, *et al*: Irbesartan overcomes gemcitabine resistance in pancreatic cancer by suppressing stemness and iron metabolism via inhibition of the Hippo/YAP1/c-Jun axis. J Exp Clin Cancer Res 42: 111, 2023.
89. Dhanaraman T, Singh S, Killoran RC, Singh A, Xu X, Shifman JM and Smith MJ: RASSF effectors couple diverse RAS subfamily GTPases to the Hippo pathway. Sci Signal 13: eabb4778, 2020.
90. Sayedyahossein S, Babu Sait MR, Li Z, Banerjee R, Tran A, Thines L, Karimi M, Bahmani M, Mishan N, Borzou P, *et al*: KSR1 is a scaffold for the Hippo signaling pathway. Commun Biol 8: 1725, 2025.
91. Wang Y and Yu FX: Angiomotin family proteins in the Hippo signaling pathway. Bioessays 46: e2400076, 2024.
92. Gao Y, Peng Q, Li S, Zheng K, Gong Y, Xue Y, Liu Y, Lu J, Zhang Y and Shi X: YAP1 suppression inhibits autophagy and improves the efficacy of anti-PD-1 immunotherapy in hepatocellular carcinoma. Exp Cell Res 424: 113486, 2023.
93. Di Federico A, Mosca M, Pagani R, Carloni R, Frega G, De Giglio A, Rizzo A, Ricci D, Tavolari S, Di Marco M, *et al*: Immunotherapy in pancreatic cancer: Why do we keep failing? A focus on tumor immune microenvironment, predictive biomarkers and treatment outcomes. Cancers (Basel) 14: 2429, 2022.
94. Peng Q, Li S, Shi X, Guo Y, Hao L, Zhang Z, Ji J, Zhao Y, Li C, Xue Y and Liu Y: Dihydroartemisinin broke immune evasion through YAP1/JAK1/STAT1, 3 pathways to enhance anti-PD-1 therapy in hepatocellular carcinoma. bioRxiv: Nov 30, 2021 doi: 10.1101/2021.11.30.470572.
95. Shen T, Li Y, Zhu S, Yu J, Zhang B, Chen X, Zhang Z, Ma Y, Niu Y and Shang Z: YAP1 plays a key role of the conversion of normal fibroblasts into cancer-associated fibroblasts that contribute to prostate cancer progression. J Exp Clin Canc Res 39: 36, 2020.
96. Fan Y, Gao Y, Rao J, Wang K, Zhang F and Zhang C: YAP-1 promotes tregs differentiation in hepatocellular carcinoma by enhancing TGFBR2 transcription. Cell Physiol Biochem 41: 1189-1198, 2017.
97. Murakami S, Shahbazian D, Surana R, Zhang W, Chen H, Graham GT, White SM, Weiner LM and Yi C: Yes-associated protein mediates immune reprogramming in pancreatic ductal adenocarcinoma. Oncogene 36: 1232-1244, 2016.
98. Li H, Xiao Y, Li Q, Yao J, Yuan X, Zhang Y, Yin X, Saito Y, Fan H, Li P, *et al*: The allergy mediator histamine confers resistance to immunotherapy in cancer patients via activation of the macrophage histamine receptor H1. Cancer Cell 40: 36-52.e9, 2022.